Remote sensing time series analysis of waterbody colour change in Northern Canada

Genevieve George

Supervisor: Anders Knudby

Thesis Committee:

Dr. Sylvain Leblanc
Dr. Antoni Lewkowicz

Thesis submitted to the Faculty of Arts in partial fulfillment of the requirements for a Master of Science in Geography

Department of Geography, Environment and Geomatics
University of Ottawa

Abstract

This study used Landsat data from 1984 to 2021 processed in Google Earth Engine to analyze the spatial and temporal pattern of waterbody colour change in Northern Canada. We created biennial composite mosaics with the 25th percentile pixel reflectance value from all valid cloud and ice-free Landsat pixels over each two-year period from 1984 to 2021. Waterbodies were defined as groups of contiguous water pixels from the Global Surface Water dataset greater than one hectare in size. According to this definition, a total of 1,453,464 waterbodies were identified and used in this study. We defined five optical change indicators: surface reflectance in the blue, green, red, and near-infrared bands, as well as turbidity calculated from the red band. The pixel values for each waterbody were first summarized zonally into median values for each waterbody in each mosaic, and then temporally, into Mann Kendall statistic and Theil Sen slope values of each change indicator for each waterbody across all mosaics. The time series statistics for each waterbody were then used as inputs to a random forest classifier to assign a value of changed or unchanged to each waterbody in the study area. The model classified 22.9% of the waterbodies as changed, with an overall accuracy of 91.8% and an AUC score of 0.95. The change was clustered in coastal areas and several inland regions. Each changed waterbody was then assigned a year of change based on the year of greatest absolute interannual change in the time series of green band reflectance. The pattern across the entire study area showed early peaks of change in 1986 and 1994, and more recent smaller peaks of change in 2008, 2012, and 2020. The pattern of temporal change was highly variable by region. This study shows promising results for the use of remote sensing to monitor waterbody change across very large areas. Furthermore, the methods outlined in this paper for creating composite mosaics and classifying waterbody colour can be easily modified and applied to new regions.

Acknowledgements

First and foremost, I would like to thank Dr. Anders Knudby for your invaluable support. You have been encouraging, considerate, attentive, and patient beyond belief while working with me over the past few years. Thank you for your academic and non-academic support, setting me up with odd-jobs and connections that made my experience here so much richer. Thank you also for all of the imaginary deadlines; I'm sorry they didn't always work. My first piece of advice to any prospective graduate students (after "are you sure?") is "make sure you have a great supervisor". I am exceedingly grateful that I had the best one.

Thank you to my committee members, Dr. Sylvain Leblanc and Dr. Antoni Lewkowicz, for your support, inclusiveness, and for always making me feel welcome in your respective fields. Thank you to Dr. Leblanc and Natural Resources Canada for funding this research. Thank you Dr. Lewkowicz for providing the data, permafrost knowledge, and base research that this thesis is built upon. Thank you also to Dr. Lewkowicz and colleagues at PermafrostNet for inviting me and encouraging me to participate in your working groups, which provided me with important experience and a friendly environment.

Thank you to Dr. Koreen Millard who helped me orient the strange and beautiful world of Google Earth Engine, and continued to be a resource as I navigated the pitfalls of .getInfo().

I would also like to extend my thanks to my friends and peers who provided endless long chats and deeply enriched my experience. Yulun, Andrew, Kutalmis, Matus, Yiwen, Chris, Galen, Claudia, Kiyomi, Fiona, thanks for always being there. Whether it was in courses, TAing, or just around the lab, your presence made it all the better.

Finally, I would like to thank my own personal support group. Mum, thanks for *everything* but especially your unwavering presence. Rob, thank you for being my personal search engine; your knowledge, good advice, and—most importantly—patience have been my rock. To the rest of my friends and family, thank you for keeping me on track with your choruses of "have you submitted yet?". You'll all be happy to know that yes, I have now.

Table of Contents

List of Figures

List of Tables

1. Introduction

Global climate change is disproportionately affecting the Arctic, where warming is estimated to occur at nearly quadruple the rate of the global average (Rantanen et al., 2022). This warming causes rapid change to northern environments, and understanding these changes and impacts requires frequent, large-scale and accurate monitoring of the Arctic environment. This level of monitoring is challenging due to the size of the area and lack of infrastructure in the Arctic, particularly for a phenomenon like permafrost thaw that is geographically distributed and challenging to map with satellite data.

In northern Canada, thawing permafrost can impact the water quality in inland waterbodies by triggering geomorphic activity that releases sediment and organic matter downstream. This increased input of terrestrial matter can change the physical and chemical properties of lakes, which can affect trophic system dynamics, contribute to increased carbon emissions, and affect human activities that depend on clear lake water (Wauthy et al., 2018). Changes to the amount and kinds of particulate matter in lakes affects their optical properties and can lead to drastic lake colour change (Graneli, 2012). Lake colour change has been sporadically identified and studied in Northern Canada (Bouchard et al., 2014; Lewkowicz & Way, 2019; Watanabe et al., 2011), but its magnitude, as well as any spatial and temporal trends, remains unknown (Wauthy et al., 2018).

Effective monitoring of lakes is useful to understand more far-reaching implications of climate change because lakes can function as sentinels of environmental change (Williamson et al., 2008). The inaccessibility of much of Northern Canada is a challenge for Arctic scientists studying the rapidly changing landscape (Canadian Polar Commission, 2015), and the geographic distribution and remoteness of northern lakes in Canada makes large scale monitoring of lake water quality change a challenging task. In particular, the spatially and temporally limited coverage of water quality sampling, and the temporal variability of the permafrost environment, make traditional monitoring methods cost-prohibitive to apply to such a large area. However, lake colour change is a phenomenon that can be observed from freely available satellite imagery. Landsat satellite imagery has been available at 30-m resolution since the launch of Landsat 4 in 1982, and it captures data within the visible bands, making it suitable for large-scale and long-term monitoring of lake water. Landsat data can be used to detect

differences in water colour and thereby estimate specific water quality parameters such as total suspended solids, Secchi disk depth, dissolved organic carbon, chromophoric dissolved organic matter, and chlorophyll a concentration (Gholizadeh et al., 2016a).

Identifying areas that are experiencing drastic visible changes may also help provide insight into ongoing but less detectable changes (Canadian Polar Commission, 2015). For example, it is likely that changes with no optical expression, such as permafrost thaw and greenhouse gas release, are happening in tandem with lake colour change, either caused by the same environmental triggers, or as an indirect consequence of lake colour change (Williamson et al., 2008). As a result, the detection of areas of lake colour change may highlight areas undergoing broader environmental change, which could help to focus research efforts into the mechanisms and impacts of climate change in a range of scientific disciplines.

In this study we use Landsat imagery to identify the spatial and temporal trends in water colour change for northern Canadian waterbodies for the period of 1984-2021. The following sections present a review of the literature on Arctic lake dynamics, water quality monitoring, and large-scale remote sensing (chapter 2), as well as the study objectives (chapter 3), methodology (chapter 4), and the results (chapter 5), before finishing with a discussion (chapter 6) and conclusion (chapter 7).

2. Literature Review

2.1 Warming Arctic and Permafrost Thaw

2.1.1 Warming Arctic Climate

The Arctic is warming more rapidly than the global average due to the effects of Arctic amplification—a process whereby warming is enhanced relative to lower latitudes as a result of local feedback loops (Previdi et al., 2021). Rising temperatures cause sea ice to melt, thus decreasing the surface reflectance, or albedo, in the Arctic Ocean. The exposed seawater then absorbs significantly more solar insolation than would be the case under normal, ice-covered conditions, leading to further warming (McBean et al., 2005). The sensitive snow, ice, and salinity regimes in the Arctic Ocean exacerbate this process because small changes in temperature and salinity lead to further degradation of sea ice and its consequent effects (McBean et al., 2005). A similar process takes place on land, where reduced snow cover leads to increased absorption of sunlight, and hence warming. Increasing

temperatures and decreased albedo can also trigger other feedback loops that amplify warming, including permafrost degradation that can release greenhouse gases as formerly frozen organic material decomposes (Camill, 2005; Turetsky et al., 2019).

Rising temperatures and disruptions to the delicate balance of interconnected systems can cause a ripple effect in the Arctic ecosystems. For instance, direct warming and its cascading effects such as changes to freeze-thaw cycles, variations in the length of the cold season, and alterations to ice formation patterns can strongly impact biological processes (Kattsov et al., 2005; McBean et al., 2005). The Arctic's environmental systems interact in both cumulative and contradictory ways; positive and negative feedback loops often occur simultaneously making it difficult to identify individual contributions and quantify overall impacts (McBean et al., 2005). However, studies have already shown how climate change can impact Arctic ecosystems, including by disrupting organism niches and forcing migration (Finstad & Hein, 2012; Moore & Huntington, 2008), increasing competition for resources (Gilg et al., 2012; Joly et al., 2009), and threatening particularly vulnerable species with extinction (Berteaux et al., 2004).

2.1.2 Permafrost Thaw

Rapid warming in the Arctic is triggering and increasing the rate of the thawing of permafrost, ground that remains frozen for at least two consecutive years (Grosse et al., 2013). Above the permafrost is a layer of soil that freezes and thaws seasonally, called the active layer. In addition to frozen soil, areas of ice-rich permafrost also contain ice wedges that can exacerbate permafrost thaw and landscape degradation when they melt (Nelson et al., 2001). This process, and its associated land formations, are called thermokarst (Grosse et al., 2013). Sub-zero temperatures inhibit decomposition of organic material, but as the ground thaws, organic carbon can be converted into atmospheric carbon dioxide via microbial decomposition. Increasing atmospheric carbon dioxide contributes to the greenhouse effect, thus contributing to global warming and climate change. Permafrost thaw is a prominent issue in the scientific community, but there is no scientific consensus on its magnitude and severity, primarily due to lack of data (Turetsky et al., 2019).

Thaw processes are categorized based on their rate of thaw into gradual and abrupt thaw. Gradual thaw consists of a deepening of the active layer, and thus thaw of ground that has been frozen for a long

time, via slow and steady downward conductive heat flux (Schuur et al., 2008). Abrupt thaw is associated with ice-rich permafrost; as ground ice thaws, it causes ground subsidence (Nelson et al., 2001). Abrupt thaw often occurs on unstable slopes but can also occur on flat landscapes (Olefeldt et al., 2016). Though both gradual and abrupt thaw can lead to the decomposition of formerly frozen organic carbon and the release of greenhouse gases, abrupt thaw is a more serious issue because it involves the rapid release of large quantities of carbon dioxide into the atmosphere (Anthony et al., 2018).

Permafrost thaw also influences the composition of Arctic lake microbial communities, which is likely to affect the functioning of these ecosystems as the climate changes (Comte et al., 2016). Increased dissolved organic carbon (DOC) concentrations in lakes can increase microbial respiration and decrease photosynthesis because of shading leading to decreased light penetration (Brothers et al., 2014). The effects of increased DOC on freshwater systems are complicated but can lead to oxygen depletion and anoxic conditions (Brothers et al., 2014). Anoxia causes a switch from aerobic to anaerobic microbial metabolism, resulting in increased methane production (Deshpande et al., 2015). Furthermore, brownification—the colour transition toward brown as a result of increased DOC input—and anoxia are linked in a feedback loop which can drastically increase greenhouse gas surface emissions in lakes (Brothers et al., 2014).

2.1.3 Permafrost Thaw Distribution

Permafrost thaw is happening across the Arctic, but it is a non-uniform process. Permafrost areas can be classified according to their percentage of permafrost: continuous (90-100%), discontinuous (50-90%), sporadic (10-50%), and isolated (0-10%) (Brown et al., 2002). Permafrost thaw within these classes is similarly varied, with some regions thawing rapidly and other thawing slowly (Turetsky et al., 2019). These patterns of permafrost distribution and thaw are influenced strongly by latitude, and also by local factors including topography, hydrology, vegetation, snow cover, and ground composition (Olefeldt et al., 2016; Schuur et al., 2008).

Permafrost thaw caused by disproportionate warming in the Arctic is disrupting the function of connected Arctic ecosystems, including microbiological activity leading to greenhouse gas emissions. Scientists formerly hypothesized that permafrost thaw would release catastrophic amounts of

greenhouse gases to the atmosphere (Camill, 2005). Although the general consensus now is that this will happen more slowly than previously feared, permafrost thaw will still alter the Arctic landscape considerably (Anthony et al., 2018; Loiko et al., 2017). The rate of permafrost thaw varies across the Arctic, with abrupt thaw occurring primarily in thermokarst landscapes (Turetsky et al., 2019). It is estimated that 20% of the Arctic is composed of thermokarst landscapes that are vulnerable to abrupt thaw (Olefeldt et al., 2016).

Permafrost thaw is difficult to effectively monitor across large geographic extents because direct ground monitoring methods are limited by high costs and inconsistent sampling efforts (Duguay et al., 2005). However, remote sensing techniques can offer some insight into permafrost dynamics. For example, recent studies using passive microwave sensors have shown good accuracy for detecting thermal stability and identifying permafrost extent (Gao et al., 2020; Park et al., 2016). Given the right conditions, multispectral and optical remote sensing can also use land features or surface dynamics as proxies to assess permafrost extent and thaw (Fichot et al., 2013; Nitze et al., 2018; Rudy et al., 2013). Permafrost is generally difficult to monitor with remote sensing technology because it is a sub-surface phenomenon, but in certain environments, particularly thermokarst environments, where permafrost thaw releases sediment into nearby water bodies, the change in water quality is detectable by optical sensors. Space-based monitoring of changes in water colour and quality can thus act as a proxy for identifying broad spatial and temporal trends in permafrost thaw.

2.2 Large Scale Water Quality Monitoring

2.2.1 Northern Lake Monitoring

Lakes are a ubiquitous feature of the Arctic landscape, and it is estimated that 25% of the world's lakes occur at high northern latitudes (Lehner & Döll, 2004; Smith et al., 2007). The physical and chemical properties of northern lakes differ based on their underlying substrate, formation, depth, and ecology, leading to diverse lake conditions (Larsen et al., 2017). Approximately half of northern lakes are estimated to be thermokarst lakes, formed from land subsidence due to ice wedge melt (Grosse et al., 2013). Thermokarst lakes are particularly vulnerable to impacts from permafrost thaw because they form in areas of ice-rich permafrost that are prone to abrupt thaw. Though many are old, formed at the end of the last ice age, new warming is causing disruptions like retrogressive thaw slumps in areas adjacent to these lakes (Kokelj et al., 2005; Walter et al., 2007).

Large scope water quality data and monitoring efforts, both traditional and remote sensing-based, are limited in northern Canada, despite several efforts (Colombo et al., 2019; French et al., 2014; Lacelle et al., 2014; Moquin & Wrona, 2015; Roberts et al., 2017; Vucic et al., 2020). Existing studies generally focus on small regions close to existing infrastructure. Traditional methods of water quality monitoring are particularly challenging in northern and remote environments because they are labour- and travel-intensive where infrastructure is limited. There have been some efforts in recent years to develop large scale monitoring efforts, but these notably lack data in the north (Deutsch et al., 2022; Huot et al., 2019; Ross et al., 2019). Advances in remote sensing of water quality have improved monitoring efforts in remote places. Though the same challenges exist for collecting in-situ sample data as with traditional monitoring methods, remote sensing allows for the monitoring of larger areas with decreased in-situ data collection requirements.

2.2.2 Remote Sensing of Water Quality

There is a relationship between the biogeochemistry and the optical properties of water bodies that allows for indirect monitoring of water quality from satellite imagery (IOCCG, 2000). These optical properties are divided into two categories: inherent optical properties (IOPs) and apparent optical properties (AOPs). IOPs are properties of the medium alone, including scattering and absorption coefficients, while AOPs are properties of the medium given the geometry of the radiance distribution, and for example include reflectance. Both types of properties describe the interaction of a waterbody with electromagnetic radiation (EMR), the patterns of which describe the composition of the water column, but only AOPs can be observed directly with satellite imagery (Mobley, 2022).

Optically Active Water Constituents

Water both absorbs and scatters light. Water is highly absorptive in the near-infrared (NIR) and short-wave infrared (SWIR) regions of the EMR, so most of the water-leaving radiance occurs in the visible spectrum (Mobley, 1994).

The optically active constituents of water that primarily contribute to the water-leaving radiance are phytoplankton pigment concentration (Chl-a), coloured dissolved organic matter (CDOM), and total suspended solids (TSS) (Gholizadeh et al., 2016a; IOCCG, 2000; Mishra et al., 2017).

The chlorophyll pigments in phytoplankton absorb radiation primarily in the blue and red portions of the EMR spectrum (Gholizadeh et al., 2016a), with the precise absorption spectrum being dependent on the specific pigments and taxa of organisms present in the water (Millie et al., 2000). The scattering properties of phytoplankton are low relative to their strong absorptive properties (Aas, 1996).

CDOM is the light-absorbing component of dissolved organic material. CDOM absorbance increases exponentially with decreasing wavelength, such that it primarily affects reflectance values in the blue and green regions of the EMR (Gholizadeh et al., 2016a). CDOM does not significantly contribute to scattering (Dall'Olmo et al., 2009).

TSS encompasses sediment, detritus, and microorganisms in the water column, but the suspended particulates that contribute to TSS in any one situation can vary widely based on climate, substrate, and limnological and ecological processes. The absorption and scattering of TSS is dependent on the size, shape, and refractive index of the particles (Bowers et al., 2009; Bratby, 2014). Absorption by TSS increases as wavelength decreases, following a similar pattern as CDOM (Abdelrhman, 2017).

The combination of TSS, Chl-a and CDOM, in addition to the water itself, determine overall water clarity. Water clarity is commonly quantified using Secchi disk depth (SDD), an in-situ measurement technique, and turbidity, a measurement of scattering by all water constituents (Topp et al., 2020). Spectral brightness is correlated with water clarity via water quality variables including turbidity, Secchi disk transparency (SDT), Chl-a and TSS concentrations (Brezonik et al., 2005; Kloiber et al., 2002; Lathrop & Lillesand, 1986; Topp et al., 2020).

These variables are used to assess water quality in both ocean water and inland and coastal waters, but the methods and techniques for measuring them from satellite imagery depend on the complexity of the water bodies.

Case 1 and Case 2 Waters

For remote sensing purposes, water can be classified into two categories based on its IOPs: Case 1 and Case 2 waters (Gordon & Morel, 1983; IOCCG, 2000; Matsushita et al., 2012; Mobley et al., 2004;

Morel, 1988; Morel & Prieur, 1977). A current working definition by the International Ocean Colour Coordination Group (IOCCG) classifies Case 1 waters as waters where the presence of phytoplankton dominates the IOPs, so bio-optical models that ignore suspended sediment and CDOM can work well. An estimated 80% of the world's water, including most open ocean water, are Case 1 waters (Matsushita et al., 2012).

The IOPs of Case 2 waters are also substantially influenced by particles other than phytoplankton, like suspended mineral particles, and by CDOM. In Case 2 waters, these three components can vary independently of each other, which complicates how models need to consider the three elements. Case 2 waters include most coastal and inland waters (IOCCG, 2000; Matsushita et al., 2012), likely including all Arctic lakes.

Modelling Approaches

There are two primary bio-optical modelling approaches in remote sensing: empirical and semi-analytical (Topp et al., 2020). Empirical models are based on fitting a regression between in-situ measurements of water quality and band ratios or other expressions based on satellite imagery from the same time period. These models are simple but non-generalizable and so only apply to the spatio-temporal environment of the study (Kutser et al., 2001). Semi-analytical (and fully analytical) models are physics-based methods that model the inherent and apparent optical properties of the water body in order to estimate the optically active water constituents. These models are considerably more complicated, but may be theoretically generalizable beyond the scope of the study. Nevertheless, the relationships between water quality parameter concentrations and IOPs can vary locally and temporally (Kutser 2001, Giardino 2007, from Giardino 2010) in optically complex waters such as lakes, making it difficult to create universally applicable analytical models. Despite these complications, remote sensing has been used extensively to assess inland water quality since the early 1970s (Gholizadeh et al., 2016b, 2016a; Matthews, 2011; Topp et al., 2020).

Optically active water constituents, including TSS, Chl-a, and CDOM are often used to assess water quality (Gholizadeh et al., 2016a). TSS is a useful indicator of water quality because the concentration of suspended organisms and minerals contributes to primary production in the waterbody as well as to water clarity (Matthews, 2011). There is no consensus on the best bands or band ratios for identifying

TSS (Matthews, 2011) but most algorithms use the red and NIR bands (Östlund et al., 2001). Chl-a can also be an indicator of primary productivity in lakes (Matthews, 2011). Band ratios of reflectances from broad-band sensors can be used to estimate Chl-a, but there is some variability in its effectiveness. Generally, these algorithms use linear regressions of ratios of the red, blue, or NIR bands (Lathrop & Lillesand, 1986; Matthews, 2011). Absorption by CDOM is extensively used when looking at lake quality because it can be used to estimate dissolved organic carbon (DOC) by analyzing the light-absorbing fraction of DOC (which is CDOM) and then use the relationship between DOC and CDOM to estimate DOC (Hestir et al., 2015; Kutser et al., 2005; Kutser & Tranvik, 2014; Matsuoka et al., 2013; Watanabe et al., 2011). However, the relationship between CDOM and DOC is highly variable and needs to be considered when estimating DOC from remote sensing data (Hestir et al., 2015).

2.3 Lake Colour Change

There is no one kind of lake colour change, nor can it be explained by one mechanism. Different types of lakes can experience a variety of changes, dependent on their environment, substrate, formation and type. However, in Northern Canada, changes in lake colour and clarity can often be attributed to permafrost thaw (Wauthy et al., 2018). Lake water quality can be affected by terrestrial sediment that is introduced by permafrost thaw nearby or further upstream. For example, retrogressive thaw slumps adjacent to lakes have been linked to drastic lake colour change in Northern Canada (Lewkowicz & Way, 2019).

Observed lake colour changes in the Arctic span a spectrum of different colours, from clear blue to turquoise and brown (Lewkowicz & Way, 2019; Matta et al., 2017; Williamson et al., 2015). Not all of these changes can be attributed to an increase in organic material leading to a brown colour ("brownification"), but instead the colour variety suggests an overall increase in turbidity caused by both organic and inorganic substances. The extent and impacts of lake colour change are important to study, especially since the rate of change appears to be linked with warmer temperatures (Lewkowicz & Way, 2019), which are expected to continue to rise.

Water colour change is important to study because it is closely related to water quality. Differences in the colour of thaw waters have been directly attributed to variations in the concentrations of DOC and

non-algal suspended particulate matter (Watanabe et al., 2011). Lake colour has also been used as a proxy for total suspended solids using water reflectance in the NIR to categorize lake colour and estimate its sediment concentration (Matta et al., 2017). Manual inspection of lake colour in optical satellite imagery is also a useful tool to select water sampling locations for further study (Dvornikov et al., 2018).

3. Study Objectives

Given the rapid and diverse climate-driven changes experienced by northern environments, there is a need to understand the temporal and spatial scope of the ongoing changes. Numerous studies have shown clear evidence of waterbody colour change in the North, but there has been no quantification of the extent of these changes, nor of their spatial and temporal patterns. The goal of this research was to assess the spatial and temporal trends in water colour change of waterbodies in Northern Canada by answering two main research questions:

1. Can remote sensing be used to identify waterbody colour change in the Canadian Arctic?
2. What are the spatial and temporal trends in waterbody colour change across the Canadian Arctic?

These questions were answered using a big data approach, processing a large volume of Landsat satellite imagery with Google Earth Engine. An image compositing method was developed using Landsat 5-8 imagery from 1984-2021, the longest earth imaging data record with consistent spatial and spectral resolution. Band-specific surface reflectance values were summarized biennially for each individual inland waterbody across Northern Canada, defined as all territory north of the 60°N parallel. Waterbody colour was then classified as changed or unchanged using a machine learning classification based on the time series of reflectance values. This cloud-computing approach allowed for the analysis of all available Landsat imagery across the large spatial and temporal scope of the project.

4. Methodology

4.1 Study Area

For the purposes of this study, Northern Canada was defined as all Canadian territory north of 60°N (Figure 1). The 60th parallel north generally delineates the southern provinces from the northern territories, but also includes a small part of northern Quebec. There was no explicit northern boundary for the study area, however, the study area functionally excludes most waterbodies north of 75°N because multiseason ice cover prevents them from meeting the mosaicking criteria described in Section 4.2.5. The study region covers a total area of 4,010,504 km^2 and includes an estimated 1,465,826 waterbodies greater than one hectare (Section 4.2.1).

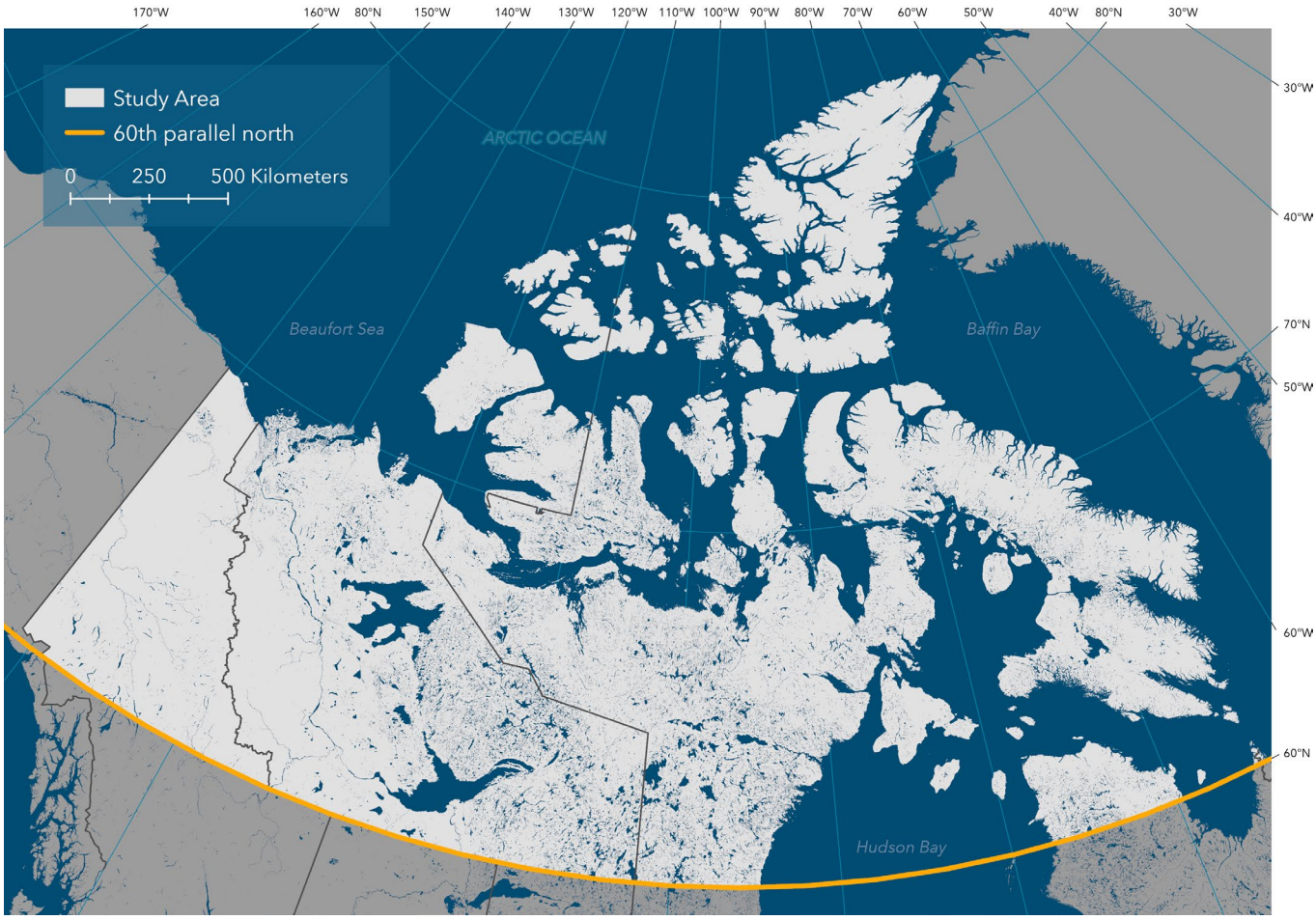

Figure 1. Study area representing all of Canada north of 60°N.

Figure 2 and Figure 3 provide geographic context for the expansive study area. Northern Canada is divided into five primary physiographic regions based on their topographic features and geology: Cordillera, Interior Plains, Arctic Lands, Canadian Shield and Hudson Bay Lowlands (Fulton, 1989)

(Figure 2). The geography of Northern Canada is also characterized by the presence of permafrost at varying extents and with varying degrees of ice content (Figure 3).

The Canadian Shield physiographic region covers 44% of the study area and contains the majority (57%) of waterbodies in the study area. Other regions with significant waterbody coverage are the Arctic lands which covers 25% of land area and contains 27% of waterbodies, and the Interior Plains which covers 14% of land area and contains 11% of waterbodies. Waterbody density decreases significantly in the other physiographic regions; The Cordillera and Hudson Bay Lowlands combine to cover 17% of the study area but contain less than 5% of the waterbodies.

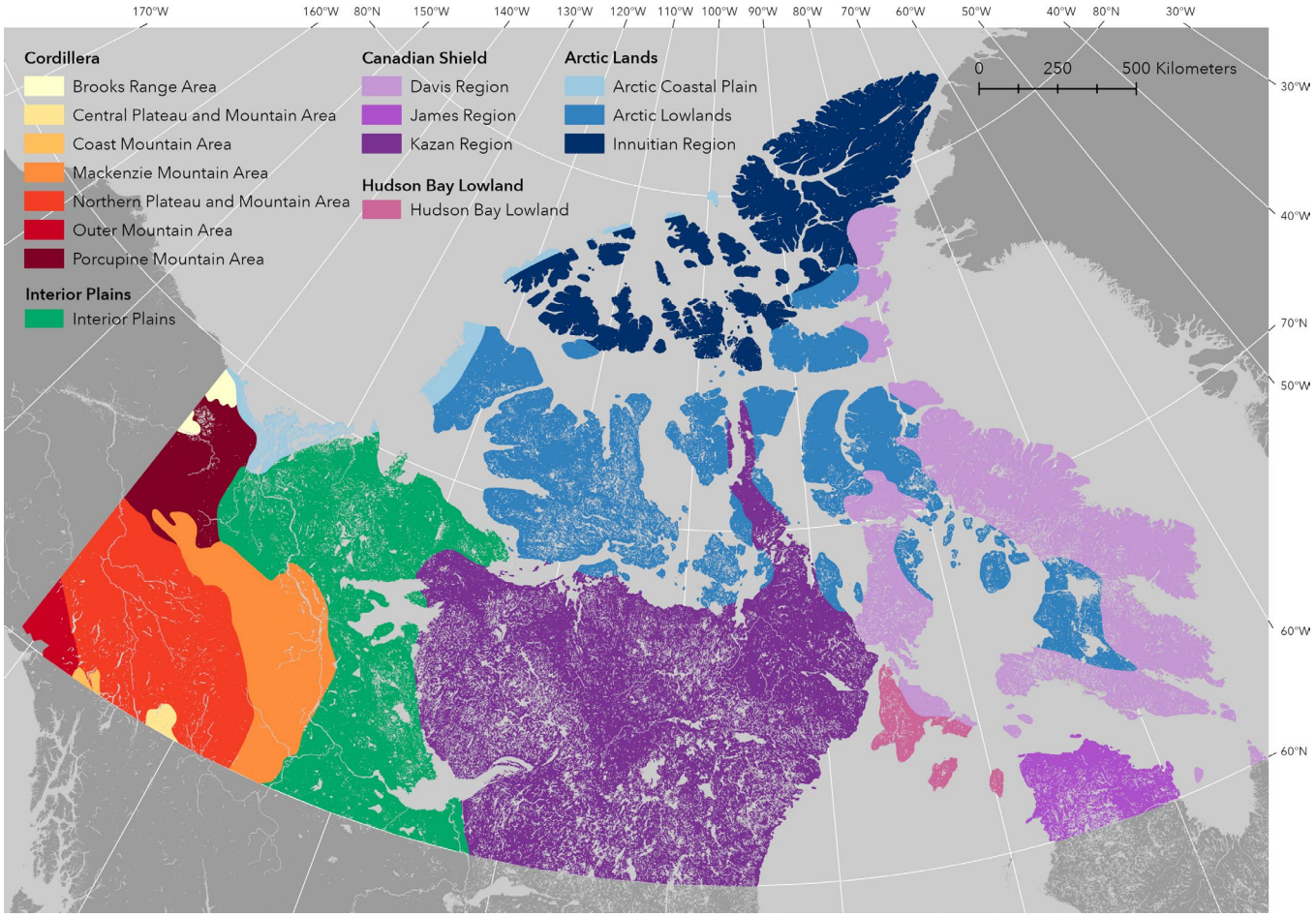

Figure 2. Northern Canada Physiographic Regions and Sub-regions within the study area. Data from Natural Resources Canada (2019).

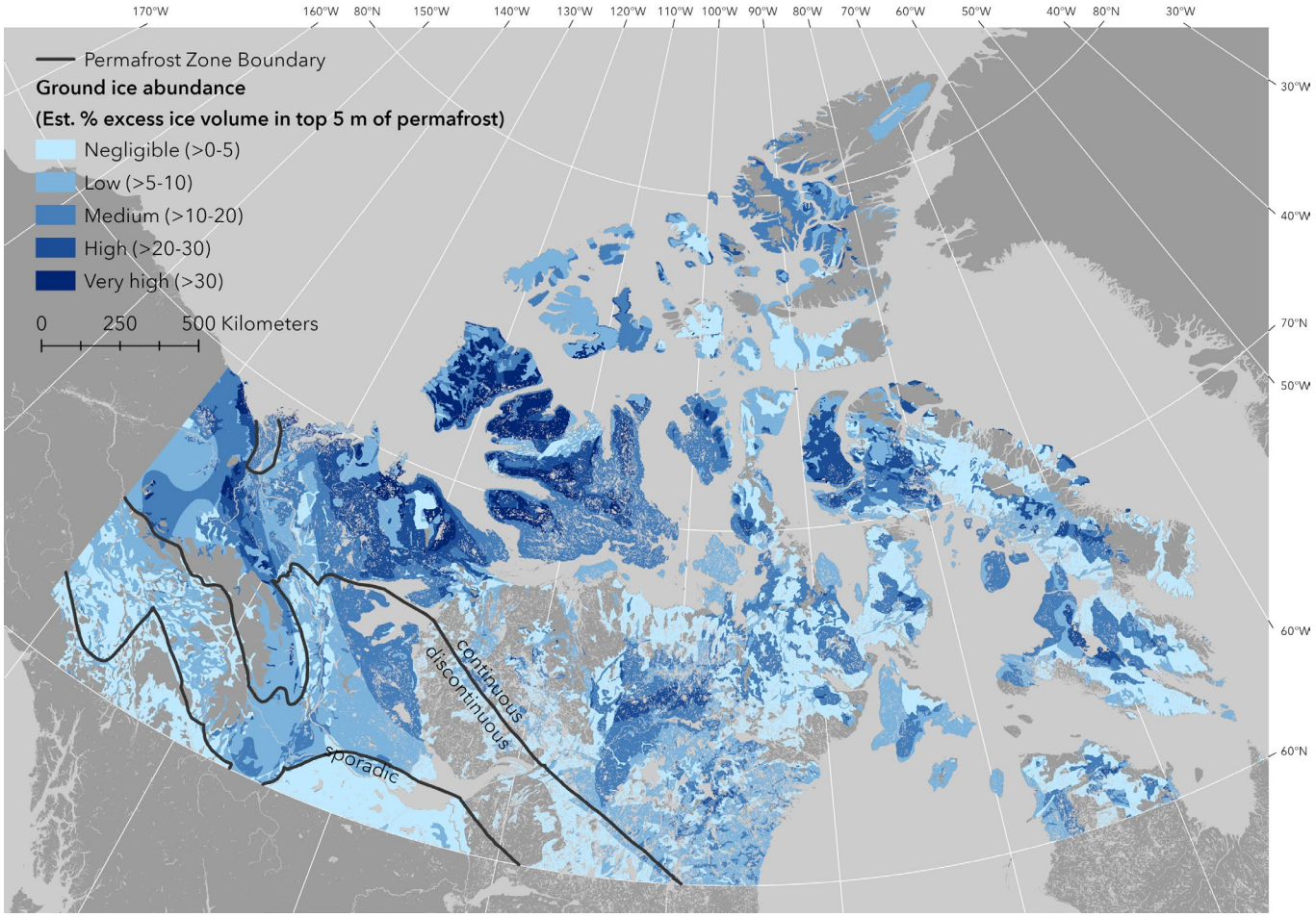

Figure 3. Permafrost extent and ground ice content for study area. Data from Geological Survey of Canada (2022).

Lake density in Northern Canada is associated with formerly glaciated terrain, permafrost presence, and peatland presence (Smith et al., 2007). The dominating lake types in Northern Canada are glacial-formed shield lakes and thermokarst lakes. The lakes formed by glaciation on the Canadian Shield represent a wide range of shapes and morphometries due to selective erosion of the resistant bedrock (Vincent & Laybourn-Parry, 2009). Thermokarst lakes are typically shallow lakes resulting from depressions formed by thawing ice-rich permafrost (Vincent & Laybourn-Parry, 2009). Other common Arctic lake types include wetland ponds, which form as a combination of surface water pooling above the permafrost barrier and poor drainage. Beyond the shield, glacial processes including erosion and sediment transport resulted in depressions that formed lake basins across Northern Canada (Vincent & Laybourn-Parry, 2009).

Northern Canada experiences long cold winters and short cool summers. Temperatures vary widely with daily average temperatures (1981-2010) ranging from -40°C in February to +6°C in July in the

high north (Eureka, NU, 79.98°N 85.93°W) and from -22°C in January to +17°C in July at lower latitudes (Fort Smith, NT, 60.02°N 111.96°W) (Environment Canada, 2022). All lakes in Northern Canada experience seasonal ice cover, with some in higher latitudes developing multi-year ice cover due to the variability and short duration of the melt season (Furgal & Prowse, 2008).

Northern Canada is very vulnerable to climate change. Within the past few decades there has been significant reductions in both spring and autumn snow cover, as well as increased permafrost temperature, altering the functioning of hydrological and ecological systems (IPCC, 2019). The patterns of permafrost thaw and decline in snow cover are expected to continue over the coming decades due to increasing surface air temperature (IPCC, 2019).

4.2 Data and Data Processing

4.2.1 Waterbody Delineations

Waterbodies were derived from contiguous regions of inland water pixels from the Global Surface Water (GSW) dataset (Pekel et al., 2016). The GSW dataset is derived from the Landsat data collection over the same time period as this study (1984-2021). Pixels in the GSW were assigned water occurrence values from 0 to 100% based on how often pixels in the Landsat collection at that location were classified as water. For this study, waterbodies were defined as groups of 8-connected contiguous pixels that have water occurrence values greater than or equal to 80% and are greater than one hectare in size. The waterbodies were then overlayed with the Canadian 2016 Census Province/Territory Cartographic Boundary (Statistics Canada, 2016) and any waterbodies that intersected with the territorial land boundary of Canada (i.e. the coastline) were removed from the analysis to eliminate bays, fjords and other coastal pixels. The Mackenzie River system, including Great Bear Lake, Great Slave Lake, and other connected lakes was classified as a single waterbody by this process, and was subsequently removed from the analysis.

This method for delineating waterbodies included primarily lakes and generally excluded river systems because their size and shape precluded them from amassing groups of contiguous 30-m pixels greater than one hectare. However, river systems or sections of rivers that met the above description were included as waterbodies and are, for the purposes of the study, functionally the same as lakes.

4.2.2 Waterbody Colour Change Data

Waterbodies delineated in the above-mentioned procedure were classified as visually having changed, or not, during the period 1984-2021 across seven areas (Figure 4 and Table 1) to train and validate a classification model. The Banks Island area uses a sample of waterbodies from across the entire island, while Areas 1-6 are rectangular regions between 116 km^2 and 385 km^2 within which all waterbodies were sampled (Table 1). Waterbodies where change type (changed or unchanged) could not be determined were removed from the dataset. Areas 2, 3, 6, and Banks Island contained many changed waterbodies, while fewer than 0.05% of waterbodies in Areas 1, 4, and 5 were classified as changed.

All waterbodies that changed between 1984 and 2016 on Banks Island (n=288) were identified, including year(s) of change, by Lewkowicz & Way (2019) based on visual interpretation of Google Timelapse imagery. Changed lakes from the Lewkowicz & Way (2019) dataset that did not coincide with waterbodies as defined in this study (see Section 4.2.1) were removed, leaving a total of 256 changed waterbodies for the Bans Island region. An additional 2% of waterbodies on Banks Island were randomly selected and classified for the entire Banks Island region to add unchanged waterbodies to the data for this area (n=323).

The rest of the waterbody colour change data was collected via visual interpretation of biennial Landsat mosaics (see section 4.3). All waterbodies greater than one hectare within areas 1-6 (Figure 4) were classified as changed, unchanged, or uncertain, in the case where a waterbody could not be confidently assigned one of the two categories. Only waterbodies classified as changed or unchanged were included in the final dataset. As with the Banks Island dataset, the year(s) when each waterbody underwent change was also recorded.

The additional six areas were chosen to supplement the Banks Island dataset based on locations where a preliminary classification model performed poorly. An initial model based on just the Banks Island dataset performed well in regions with lake changes similar to those on Banks Island, such as Victoria Island and the Bluenose Moraine area of the Northwest Territories, but performed poorly in areas with little or no water colour change, particularly in the central regions of the Northwest Territories and Nunavut. The additional areas were thus chosen to represent an increased geographic spread and increased variety of waterbody conditions from among the lake-rich regions of Northern Canada.

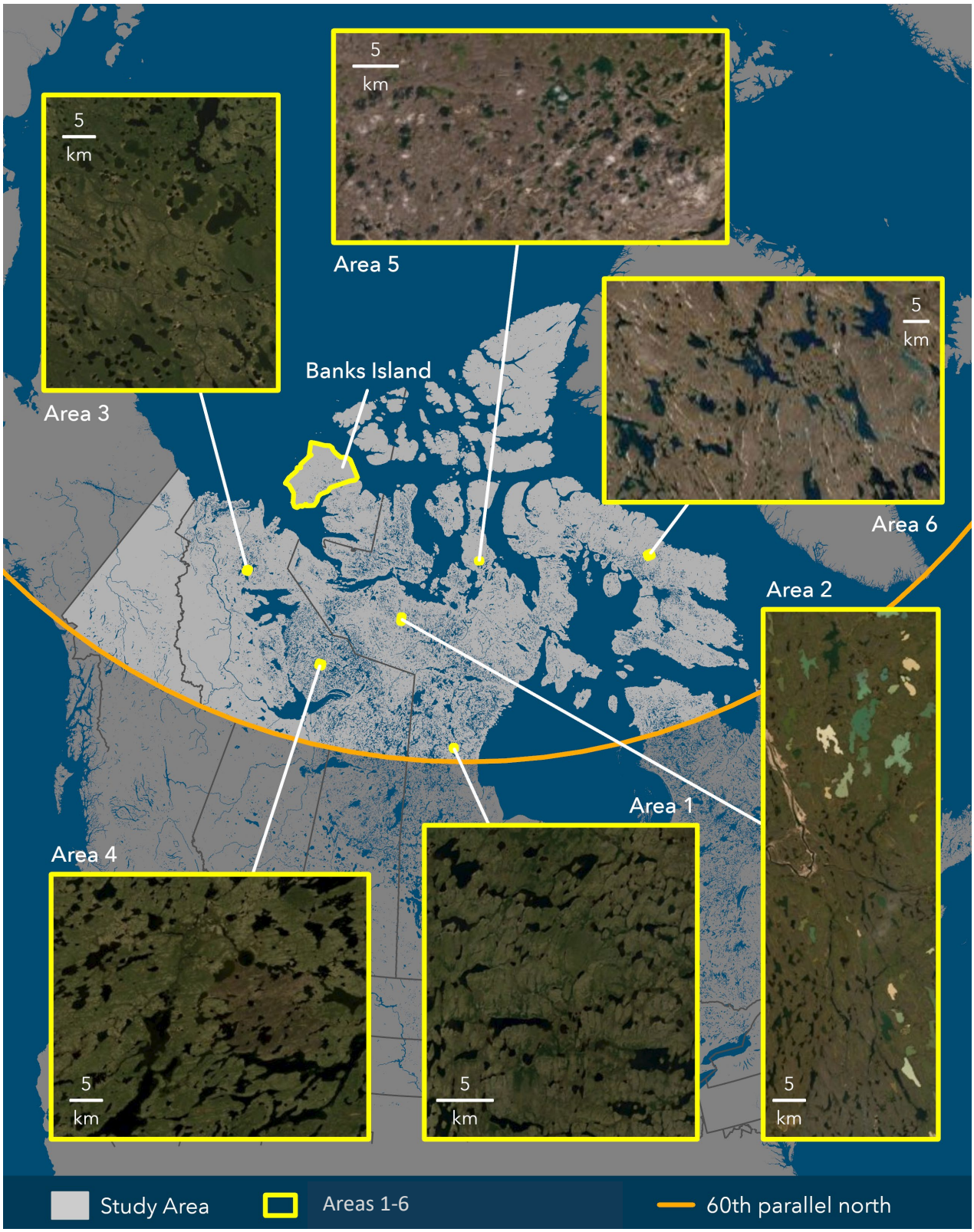

Figure 4. Areas within the northern Canada study area for which waterbodies were visually identified as changed or unchanged.

The location and environmental context for each of the areas is described below. Coordinates for Areas 1-6 correspond to the top left corner of the study area bounding box. Except where specified, all areas are located within the range of continuous permafrost.

- **Area 1 (60.75°N 97.35°W):** Located in southern Nunavut, Area 1 is the southernmost training and validation area. It is located on the Canadian Shield physiographic region within the Taiga Shield ecoregion. The permafrost in this region has medium ice content. The waterbodies are primarily dark blue in colour, indicating clear water.

- **Area 2 (67.07°N 104.50°W):** Area 2 is located in northern mainland Nunavut, in the southwest region of Queen Maud Gulf Bird Sanctuary. This area is within the Canadian Shield physiographic region. The permafrost in this region has low ice content. The waterbodies range in colour from dark blue to turquoise, to light brown, representing a range of turbidity levels.

- **Area 3 (67.22°N 125.70°W):** Area 3 is located in northern mainland Northwest Territories, north of Great Slave Lake and east of Colville Lake. This area is located in the Great Bear Plain within the Interior Plains physiographic region, on the border between the Southern Arctic and Taiga Plains ecoregions. The permafrost in this region has medium ice content. It has rolling terrain and is characteristic of a tundra ecosystem. The waterbodies are primarily dark blue in colour, indicating clear water.

- **Area 4 (64.01°N 113.32°W):** Area 4 is located in central Northwest Territories, north of Yellowknife and west of MacKay Lake within the Canadian Shield physiographic region within the Taiga Shield ecoregion in a transition area between continuous and discontinuous permafrost. The permafrost in this region has low ice content. The waterbodies of this area are primarily dark blue with a few dark green waterbodies, indicating mostly clear water.

- **Area 5 (70.08°N 94.21°W):** Area 5 is located on the southern portion of the Boothia Peninsula in northern Nunavut, within the Canadian Shield physiographic region and Northern Arctic ecoregion. The permafrost in this region has low ice content. The waterbodies of this area are primarily dark blue with a few dark green waterbodies, indicating mostly clear water.

- **Area 6 (68.62°N 70.24°W):** Area 6 is located in central Baffin Island in northeastern Nunavut within the Canadian Shield physiographic region and the Northern Arctic ecoregion. The permafrost in this region has low ice content. The waterbodies in this area are primarily dark blue, indicating clear waters, with some lighter turquoise waterbodies, indicative of higher turbidity.

- **Banks Island (73°N 121°W):** Banks Island is located in the Arctic Lands physiographic region and covers both Arctic Coastal Plain and Arctic Lowlands physiographic subregions. All of Banks Island is within the Northern Arctic ecoregion. Banks Island is characterized by rolling terrain underlain by ice-rich permafrost (medium to medium-high ice content). Waterbodies in this region range in colour from dark blue to turquoise to brown. The majority of the waterbodies are dark blue and unchanged but there has been notable colour change in waterbodies across Banks Island in recent years (Lewkowicz & Way, 2019).

The areas span a range of latitudes, from 60.6°N in Southern Nunavut to the northern tip of Banks Island at 74.5°N, to increase the diversity of waterbody images and ensure the dataset is representative of the entire study area. There are no areas in the high north or far west of Northern Canada because lake density decreases significantly farther north in the Canadian Arctic Archipelago, north of Banks Island, as well as west, toward the Cordillera physiographic region.

Table 1. Size and number of classified waterbodies present in each of the seven areas. Classified waterbodies are those that could be assigned a value of changed or unchanged based on visual interpretation of their colour from 1984-2021.

Sample Area	Area (km^2)*	Number of Classified Waterbodies	Median Waterbody Size (ha)
Area1	153	102	5.85
Area2	340	235	4.45
Area3	255	205	3.79
Area4	385	155	7.00
Area5	116	134	2.78
Area6	375	158	2.85
Banks Island	70,028**	579	5.67

* Values rounded up to nearest whole number

** A small number of waterbodies were sampled from across all of Banks Island whereas for other areas, all waterbodies within the area were sampled.

4.2.3 Landsat Imagery

Freely available Landsat imagery from Landsat missions 5 (TM sensor), 7 (ETM+ sensor), and 8 (OLI sensor) covering the period from 1984 to 2021 was used to assess the temporal trend in waterbody colour. Landsat has previously been used to assess inland water quality due to its suitable spatial resolution of 30-m, spectral resolution consisting of 7 to 11 bands consistently covering blue (~0.45 μm) to shortwave infrared (~2.3 μm) wavelengths, and long time-series of freely available data (Gholizadeh et al., 2016b; Matthews, 2011; Olmanson et al., 2008; Pahlevan et al., 2019; Wulder et al., 2019; Zhu et al., 2019). The amount and the temporal span of Landsat imagery makes it particularly useful for long-term change detection studies (Wulder et al., 2012). The Landsat archive at 30-m resolution (Landsat missions 4-8) extends from 1982 to the present, and both recent and archived imagery became freely available in 2008, making it easier to move away from scene-based analyses and utilize all available data in time series analyses (White et al., 2014; Woodcock et al., 2008; Wulder et al., 2012).

This study used Landsat Surface Reflectance imagery available through Google Earth Engine from the United States Geological Society (USGS) archives. Landsat imagery was classified into tiers based on the quality of their radiometric and geometric correction. The surface reflectance imagery was generated from Tier 1 imagery, using the LaSRC and LEDAPS atmospheric correction algorithms for Landsat 8 and Landsat 4-7 imagery respectively (USGS, 2020a, 2020b). Tier 1 products are radiometrically corrected and geometrically corrected to within a root mean square error (RMSE) of ≤12 m by the USGS (USGS, 2019). Using surface reflectance imagery limited the need for additional pre-processing and allowed for multi-sensor composite images to be created for this study (Pasquarella et al., 2016; Loveland and Dwyer 2012; Markham and Helder 2012). We did not perform any additional pre-processing, including normalization across the Landsat sensors because water colour is derived primarily from the visible bands, for which changes in sensor response relatively small (Roy et al., 2016). All suitable surface reflectance images from the Landsat archive were combined into an image collection for the creation of multi-year pixel composite mosaics.

4.2.4 Pixel-Based Image Compositing

Pixel-based image compositing is an alternative to the scene-based analyses used in traditional remote-sensing studies. In areas like Northern Canada, with a limited season of usable imagery and frequent

cloud presence (Stow et al., 2004), composite imagery allows for better analyses by combining pixels from different scenes to create a single high-quality image composite. Such image composites are created by applying a series of rules that determine which pixel, from the stack of suitable pixels from imagery covering a given time period, should be used for the composite.

Pixel composite mosaics were created for two-year periods spanning 1984 to 2021 (e.g. one mosaic is composed of pixels from 1984 and 1985, another from 1986 and 1987, etc.) across Northern Canada using the Surface Reflectance products from Landsat TM, ETM+, and OLI sensors available in Google Earth Engine. Image collections were compiled from all available Landsat imagery and filtered to eliminate unusable pixels. Images with cloud cover over 70% of the image were filtered out to eliminate error from geometrically incorrect images due to obscured ground control points (White and Wulder 2013). All images were masked for cloud and ice using the CFMask algorithm (Foga et al., 2017) and pixels with negative values in any band were also masked out. The best pixel was then extracted from the remaining pixel stacks to create the composite image, and pixels with no valid observations were masked out of the returned image.

Many studies using pixel composites select the best pixel as the one with the highest NDVI value (Van Doninck & Tuomisto, 2017). However, NDVI is not suitable as a compositing criterion for all landscapes, and especially not for water surfaces. Other methods for selecting the best pixel include using scores for sensors, day of year, distance to cloud or cloud shadow, opacity, or statistical calculations of the median or medoid (Flood, 2013; Roy et al., 2009; White et al., 2014). This study used the 25^{th} percentile of the surface reflectance value to determine the most suitable pixel for the composite mosaic images. The 25^{th} percentile value was calculated for all bands separately and combined into an aggregate pixel. The resulting pixel thus did not necessarily originate from any one image, but was created by combining the 25^{th} percentile reflectance values from each band. The 25^{th} percentile was chosen in lieu of the median because of the high likelihood of inclusion of pixels with unusually high surface reflectance, mostly from residual snow and ice. The use of the 25^{th} percentile served to eliminate pixels with ice and snow (frequent, high reflectance) as well as pixels that are dark due to cloud shadows (rare, low reflectance) and thus depict typical surface reflectance in ice-free conditions. The optimal percentile value can vary geographically based on the distribution of surface reflectance values within the image collection for a given pixel. High-latitude and high-altitude regions

may benefit from a lower reflectance percentile (~10%) because of the higher likelihood of including very bright snow and ice pixels in the imagery collection, thus biasing the reflectance distribution toward bright pixels. Conversely, sloped areas may benefit from a higher percentile (>25%) to avoid the inclusion of shadows, which reduce the amount of light reflected off the surface and could bias the distribution toward darker pixels. However, substantial visual inspection of image composites across a range of environments in the study area showed that the 25th percentile is a compromise that works well for the majority of Northern Canada.

4.2.5 Image mosaics

Figure 5 shows the mosaics of the colour change dataset for Area 2, an area in northern Nunavut. Overall, the results for the 25th percentile pixel compositing method are very good, as they succeed in creating imagery that is free of clouds, snow, ice, and shadows. However, some regions in certain mosaics have missing pixels. The 1984-1985 mosaic from Figure 5 is missing more than half of the pixels, and the 1986-1987 mosaic is missing some water pixels, which is consistent with the pattern shown in Table 2 where there are more missing pixels in earlier mosaics. These problems are the result of a lack of cloud-free and ice-free imagery, likely due to particularly cold or cloudy conditions, combined with a general lack of imagery due to poor temporal resolution of Landsat acqusitions in that period. However, the brightness of each of the images created from the 25th percentile reflectance pixels for each time period is largely consistent, making them suitable for change detection.

Figure 6 shows the number of valid pixels used to create each of the mosaics. Valid pixels come from any images in the area with no masked pixels (cloud, ice, negative values). Figure 6 shows that there are generally more pixels in later years as temporal resolution improves, particularly with the launch of Landsat 7 in 1999 and when Landsat 8 replaced Landsat 5 in 2013. There are also generally more pixels in the southern areas of the study area, where there is likely less cloud and ice, and the high northern areas, where the orbits converge and improve the temporal resolution. This is particularly true for the northernmost point of the Arctic Archipelago where there are no valid pixels in early mosaics but the highest numbers of valid pixels toward the end of the time series. In comparison, the more central latitudes of the study area, around the southern islands of the Arctic Archipelago, have generally fewer valid pixels across the time periods.

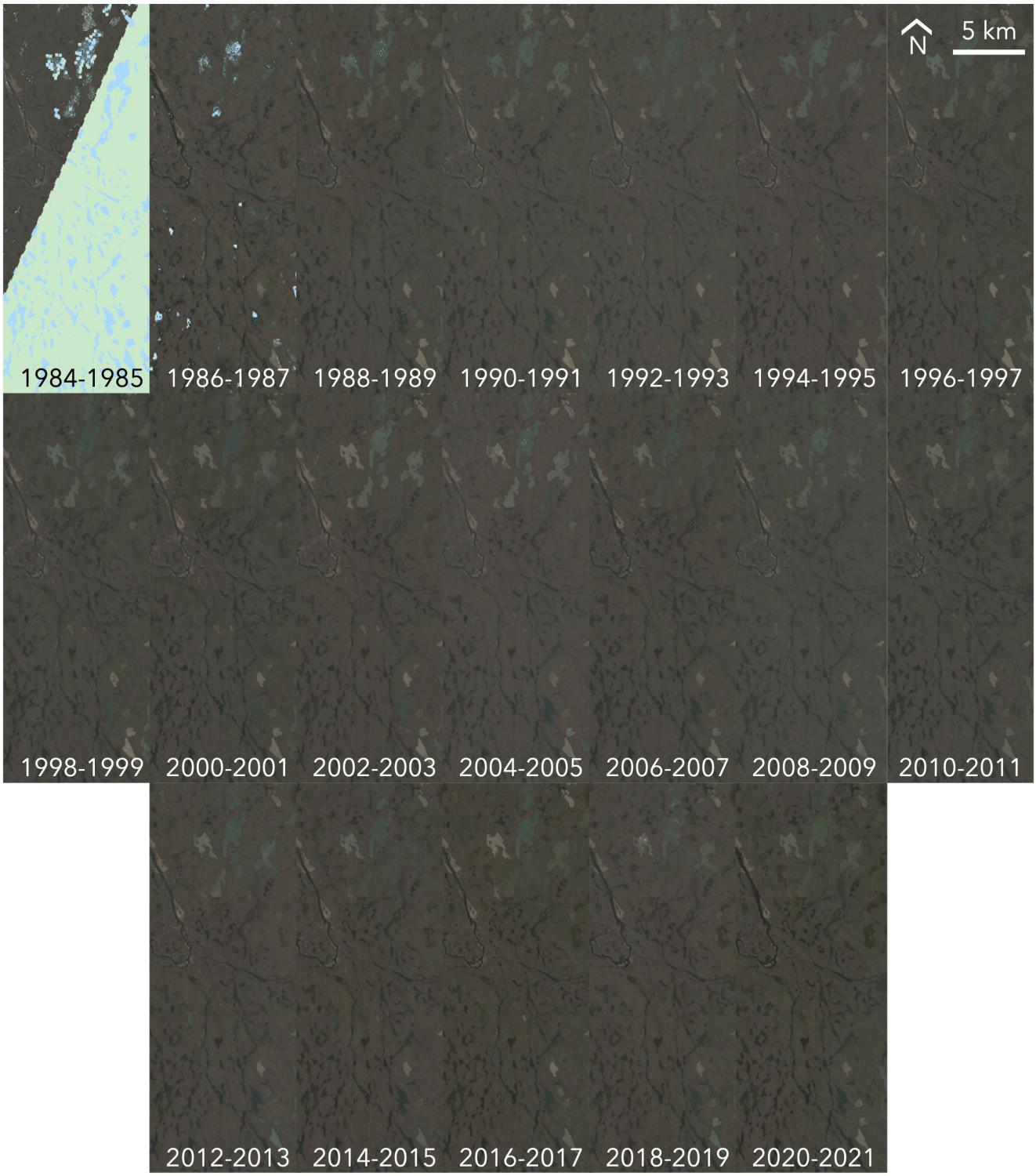

Figure 5. Biennial mosaics from 1984 to 2021 for Training Area 2 (Lat: 67.07, Lon: -104.50).

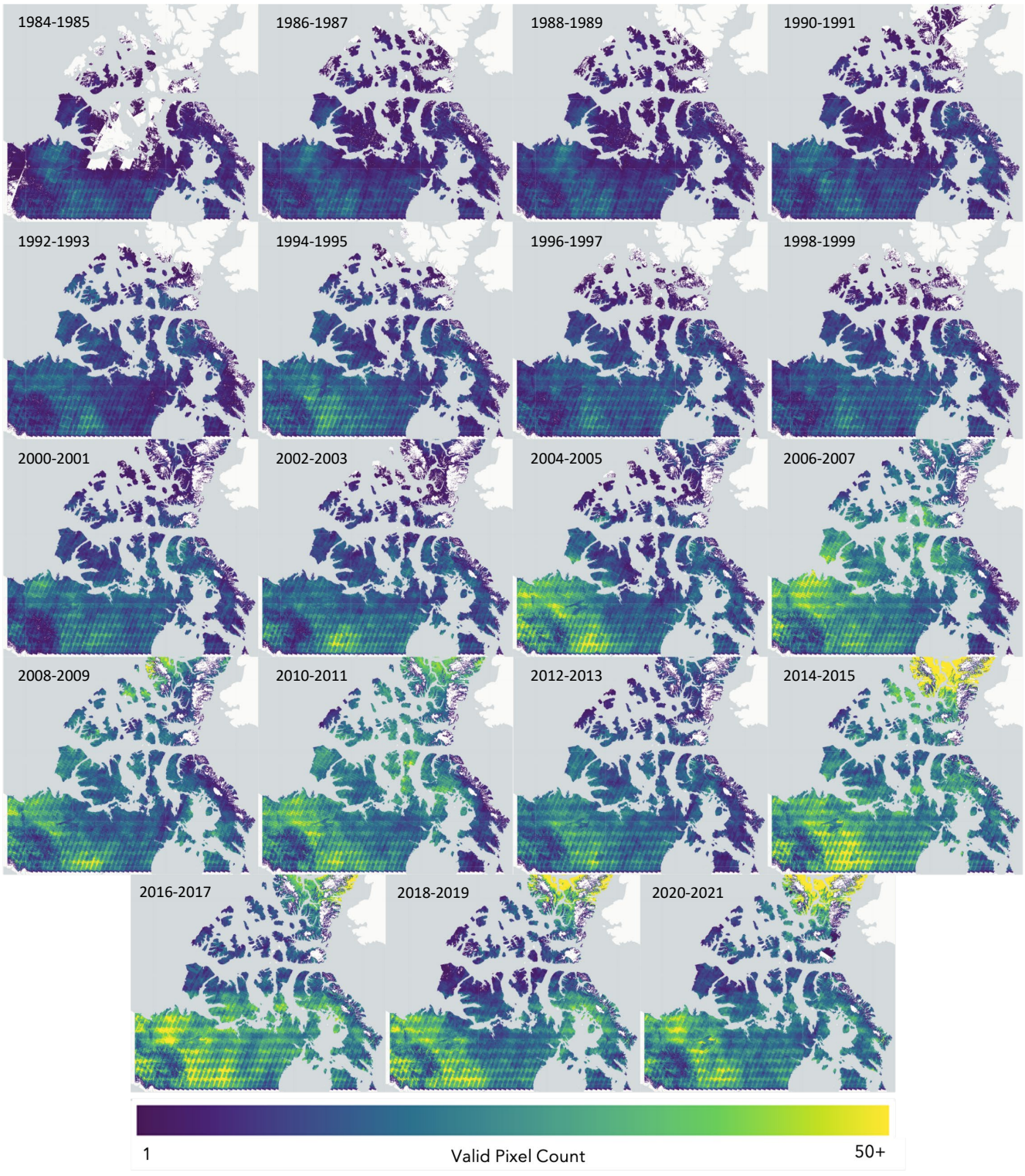

Figure 6. Valid pixel count used to create final mosaics for all biennial mosaics.

Figure 7 shows the variability in mosaic quality for a waterbody classified as changed from the northern coast of Somerset Island, Nunavut. The mosaic quality is more variable in the high north due to a reduced quantity of images (Figure 6) and thus increased likelihood of inclusion of icy pixels.

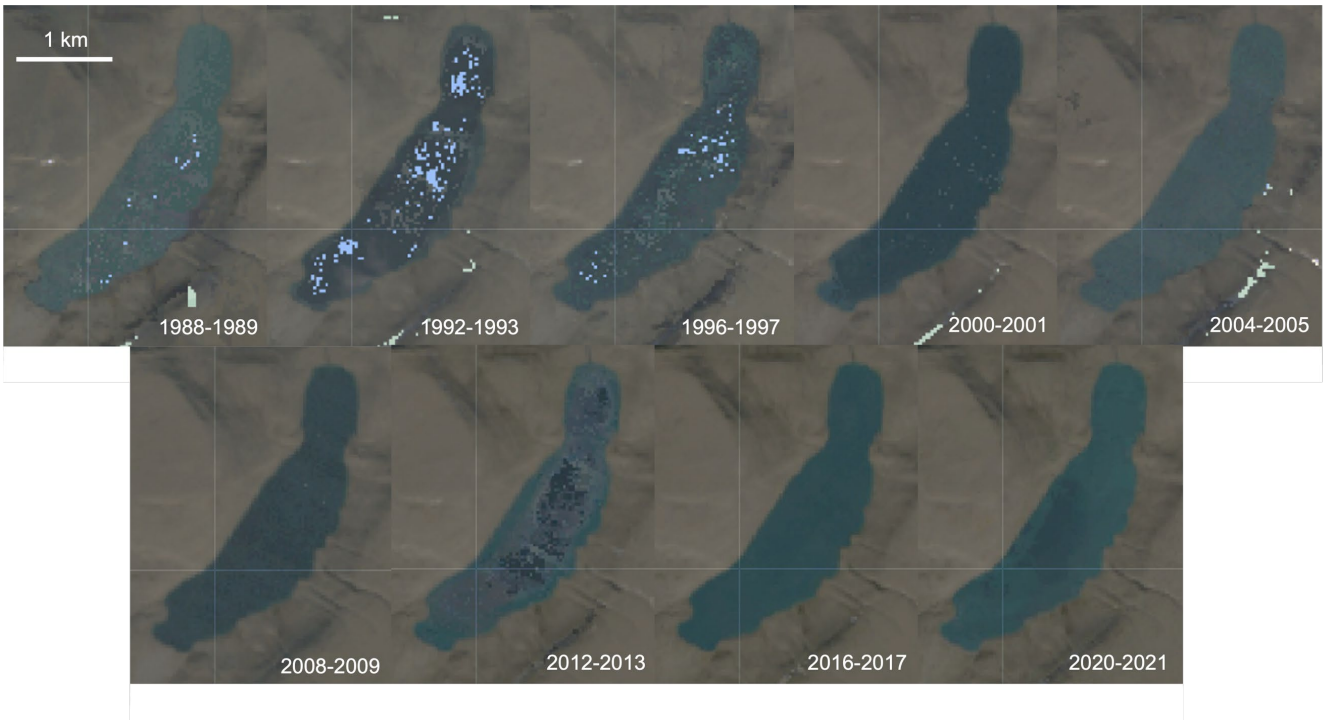

Figure 7. Shortened time series of colour-changed waterbody from northern Somerset Island, Nunavut. Every-other mosaic was excluded for clarity. Mosaic variation in the high north is more variable and some images appear to include pixels with a thin layer of ice over the water (2012-2013). Lat: 73.927, Lon: -92.263.

Table 2 shows the percentage of pixels in each mosaic compared to the total water pixels for the same area derived from the GSW dataset. Areas with no usable pixels from all imagery for the two-year time period, i.e. pixels that were not masked out from cloud or ice, show as blanks in the mosaics. The number of missing pixels in each mosaic is highest in the earlier years and decreases considerably in the later years to less than 0.6% for all of the mosaics created with imagery after 1997. The highest percentage of missing pixels is in the 1984-1985 mosaic where approximately 15% of the water pixels were masked out. Other notable mosaics with missing pixels are the 1986-1987 and 1990-1991 mosaics, which are missing 5.5% and 2.3% respectively.

Table 2. Percentage of each mosaic with valid pixels relative to the spatial cover of the Global Surface Water dataset for the same extent. The total number of pixels in the Global Surface Water dataset for the study area was 1.098 billion.

Mosaic Time Period Start	Mosaic Time Period End	Percentage of Usable Water Pixels
1984	1985	84.16%
1986	1987	94.48%
1988	1989	98.56%
1990	1991	97.66%
1992	1993	98.55%
1994	1995	99.41%
1996	1997	98.96%
1998	1999	99.42%
2000	2001	99.74%
2002	2003	99.71%
2004	2005	99.50%
2006	2007	99.78%
2008	2009	99.80%
2010	2011	99.78%
2012	2013	99.77%
2014	2015	99.91%
2016	2017	99.91%
2018	2019	99.73%
2020	2021	99.91%

Any waterbodies that were missing all pixel values for more than one year (0.8% of all waterbodies) were excluded from the subsequent time series analysis, leaving a total of 1,453,464 waterbodies included in the analysis. These lakes were primarily located in the very high north (north of 75°N) where multi-year ice was most prevalent.

4.2.6 Water Colour Change Indicators

This study uses turbidity, estimated using an existing algorithm (Eq. 1) (Dogliotti et al., 2015; Nechad et al., 2009) and surface reflectance in the blue, green, red, and NIR bands as change indicators to assess waterbody colour change derived from the pixel-composite images.

Observable water colour change manifests itself as a change in brightness, where the transition from clear blue waters to murkier water results in a change in reflectance from darker to brighter, and vice

versa. This change can be the result of diverse waterbody processes that change the composition of optical waterbody components including CDOM, TSS, and Chl-a. Studies have shown that both pixel brightness and turbidity are correlated with these optically active water constituents (Brezonik et al., 2005; Topp et al., 2020). Furthermore, the colour changes are detectable in true-colour imagery and are thus observable in the surface reflectance change of the visible light bands of blue, green, and red.

$$T\ [FNU] = \frac{A\ \rho_w(\lambda)}{1 - \frac{\rho_w(\lambda)}{C}} \qquad (Eq.1)$$

Where $\rho_w(\lambda)$ is the surface reflectance value in the red band, A = 289.29 and C =0.1686 based on a wavelength of 655nm, and FNU (Formazin Nephlometric Unit) is a standard turbidity unit.

The median values of each of the five change indicators were calculated for each waterbody in each mosaic, so that each waterbody had 95 indicator values associated with it—one value for each of the five change indictors across the 19 biennial mosaics.

4.3 Analysis

4.3.1 Change Analysis

The values of the change indicators were aggregated over the time series to assess the trend in spectral reflectance and turbidity for each waterbody over time. The time series for each change indicator across each waterbody was summarized using the original Mann-Kendall test from the pymannkendall package (Hussain & Mahmud, 2019). The Mann-Kendall test is used to detect monotonic trends, i.e. whether data in a time series is continuously increasing or decreasing. Its test statistic ranges from -1 to +1, indicating the direction and strength of a trend (how consistently they increase or decrease), with an associated p-value indicating the trend's significance, and is commonly used to assess long-term trends in satellite imagery (De Beurs & Henebry, 2004; Erasmi et al., 2014; Fraser et al., 2014; Olthof et al., 2015). The Theil-Sen slope is the median of slopes of all lines through paired points that represents the magnitude of the linear trend (how much it changes) over the given time period and is thus often accompanied with the Mann Kendall test to provide a fuller understanding of the trend. After this aggregation, each waterbody has 25 values associated with it: the Mann-Kendall statistic, its

associated p-value and variance, and the Theil-Sen slope and intercept for each of the five change indicators.

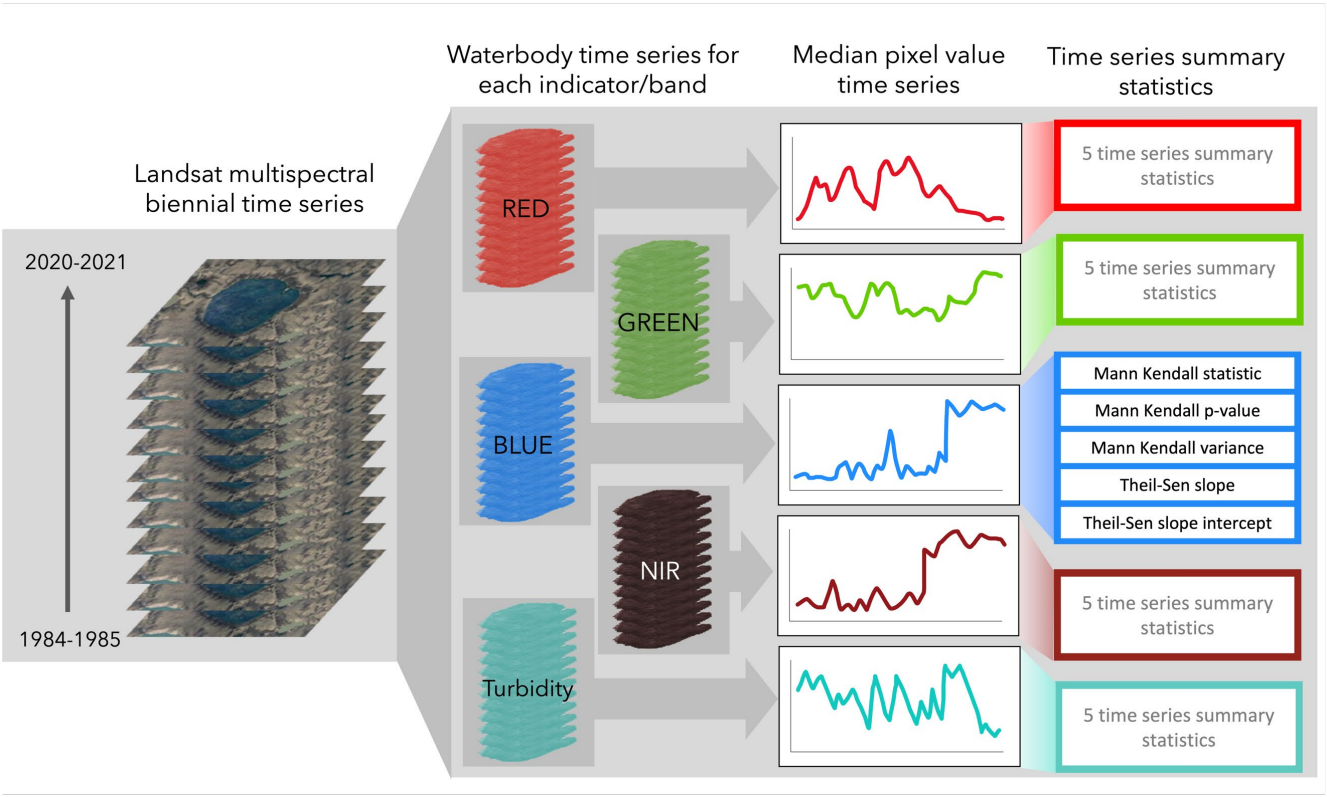

Figure 8. Concept diagram of methodology from time series mosaics to the five time series summary statistics for each change indicator (red, green, blue, and near-infrared bands and turbidity). The five time series summary statistics applied to each band are expanded in the figure for the blue band.

4.3.2 Random Forest Machine Learning Binary Classification

The visible changes in waterbody colour across the study area encompass an enormous variety of time series trajectories and patterns, best suited to distinction by machine learning supervised classification. This study used the random forest algorithm to classify waterbodies as changed or unchanged based on the summary time series values of each change indicator.

The random forest classifier is a non-parametric machine learning classification algorithm comprised of an ensemble of decision trees that averages the results of individual trees (Breiman, 2001). Each decision tree is built using bootstrap aggregating (bagging) of the training data and feature randomness. Bagging is the process of selecting a sub-sample of the training data with replacement, i.e. each waterbody is added to the subset independently from the other waterbodies of the subset, so

an individual waterbody may appear more than once in the subset for a given tree. Feature randomness is the random selection of a defined number of model variables, in this case the time series values for each band, used to determine the best splitting rule at each node in each tree. The random forest classifier has been widely used for landcover classification with time series of satellite imagery (Jin et al., 2018; Labuzzetta et al., 2021; Nitze et al., 2015; Noi Phan et al., 2020; Tatsumi et al., 2015).

The waterbody colour change data from the areas described in section 4.1.2 was split 70/30, with 30% of the data set aside for testing and 70% used for model training and validation. The 70% used for training and validation was split again, with 70% of the data for training and the last 30% for validation. Each split was stratified by class and training region to preserve the percentage of samples belonging to each class/region.

The training and validation data were used to optimize the random forest hyperparameters (the number of trees in the forest, the number of features tested at each node, and the maximum tree depth) by iteratively testing a range of values for each and selecting the parameters that showed the best results against the validation data.

Once the parameters were optimized, the model was retrained on the combined training and validation data, and the test data was used to assess the accuracy of the model.

4.3.3 Temporal Analysis

The year of change is useful in assessing whether there are any patterns in the timing of waterbody colour change. For example, particularly warm years have been shown to be associated with higher occurrence of waterbody colour change on Banks Island, associated with increased permafrost thaw activity (Lewkowicz & Way, 2019). However, some waterbodies experienced multiple periods of abrupt change, or continuous change, resulting in noisy time series with no clear way to always attribute change to a single year. To eliminate noise and to simplify the results, changed waterbodies are nonetheless assigned a single year of change, determined as the year with the maximum magnitude of interannual change in the reflectance of the green band.

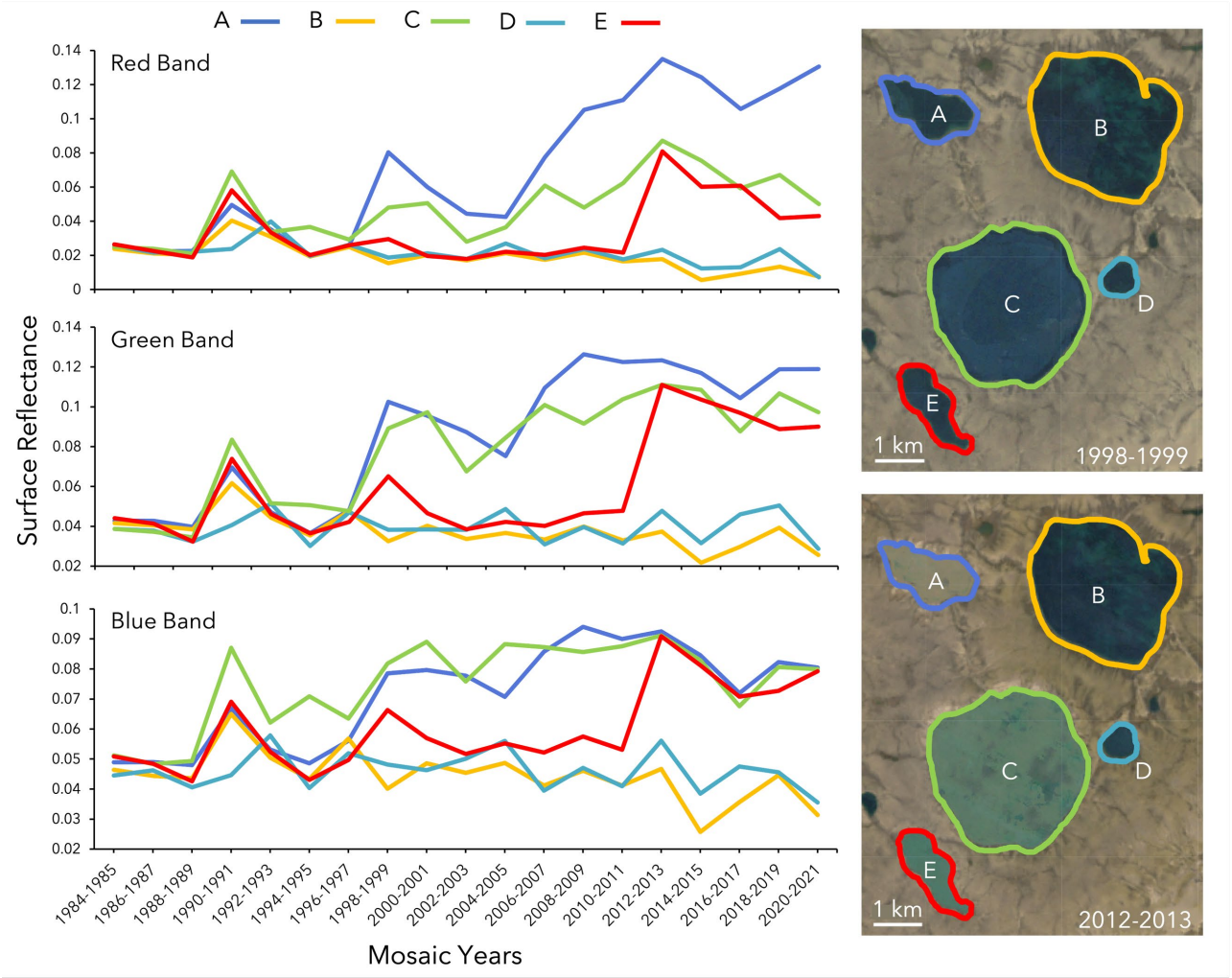

Figure 9. Time series of median surface reflectance values for five waterbodies on Banks Island (118.05°W 72.96°N) in the visible bands: red, green, and blue.

The green band was used because its temporal pattern of change aligned most closely with changed waterbodies in preliminary analyses (Figure 9). The preliminary analyses for this study considered waterbodies on the eastern coast of Banks Island that were identified as changed in Lewkowicz & Way (2019) and plotted their reflectance values in the three visible bands to ascertain whether the change could be identified in the time series graphs of red, green and blue reflectances. All three visible bands showed similar patterns for the five waterbodies, where reflectance increases as waterbodies change to brighter colours (brown for waterbody A and turquoise for waterbodies C and E) indicating that each of them could be a useful single indicator of waterbody change for changed waterbodies. However, visual examination of the time series patterns for the waterbodies across Banks Island (example

waterbodies in Figure 9) indicated that the green band is the most suitable for identifying the year of greatest change. In Figure 9, the red band can also be used to distinguish between the three different colour profiles shown in the 2012 mosaic (dark blue for waterbodies B and D, turquoise for waterbodies C and E and brown for waterbody A), however earlier in the time series around the early 2000s, it does not differentiate well between the dark blue waterbodies and the changed waterbodies, while the green and blue bands do. The blue and green bands generally show similar time series patterns, but the difference in reflectance for the different coloured waterbodies cover a larger absolute range (0.02 to 0.12) in the green band than in the blue band (0.03 to 0.09), making it easier to visually identify the change.

To assess the suitability of this method, the year of maximum interannual change from the surface reflectance time series was compared to the list of years recorded as change years in the Banks Island training data from Lewkowicz et al (2019), which were summed over the same two-year periods as the mosaics used in this study. The magnitude of change could not be reliably determined by visual examination of the image time series so all change years were included for comparison, rather than attempting to use the year of greatest change identified visually. Banks Island was the only area used to assess the viability of this method of temporal analysis because the waterbody changes on Banks Island were clear and abrupt with visually obvious differences in colour from one image mosaic to the next. The other areas were excluded from this comparison because the waterbody colour change occurs more gradually across years, making it difficult to unambiguously assign a single year of change to a given waterbody.

Figure 10 compares the automatic detection of the year of greatest change with visual detection of all years of change for each waterbody. The manual method had a greater overall number of waterbodies because it includes all years where a waterbody visibly changed (n changes = 384) whereas the automatic method included only the single year of greatest changes (n changes = n waterbodies = 316). Both methods identified the same two years of most change, 1998 and 2012, which demonstrates that the automatic detection method matched well with the visual detection of waterbody colour change on Bank's Island. However, there are also notable discrepancies in Figure 10 between the automated and manual methods of identifying year of change. The automated method identified waterbody changes early in the study from 1990-1994 that are not reflected in waterbodies identified as changed by

manual detection. The incongruency in early years was likely due to differences in the methods of handling missing pixels, which differed between the mosaicking done in this study and in Google Timelapse, used by Lewkowicz et al. (2019) to manually identify waterbody change on Banks Island. In this study, biennial mosaics were created to maximize the usable data and areas with missing pixels left with no data, while in Google Timelapse missing pixels for a given year are interpolated between valid image years (Sargent et al., 2013). The Google Timelapse methodology is visually pleasing but can be misleading, suggesting no change when change is present because the pixels in the image were derived from other years. This is particularly true for areas with many missing pixels for certain years, such as Northern Canada. Another notable discrepancy between the two methods is between 2006 and 2010, where the manual method identified the most changed waterbodies in 2006, with fewer in the next few years, while the automatic method identified the most changed waterbodies in 2008. This discrepancy could be due to the two methods not making a direct comparison; the manual method included all changes for waterbodies while the automatic method included only the largest magnitude change, essentially ignoring other changes. Thus, if a waterbody changed in 2006 but changed more in 2008, the automatic method would only record change in 2008.

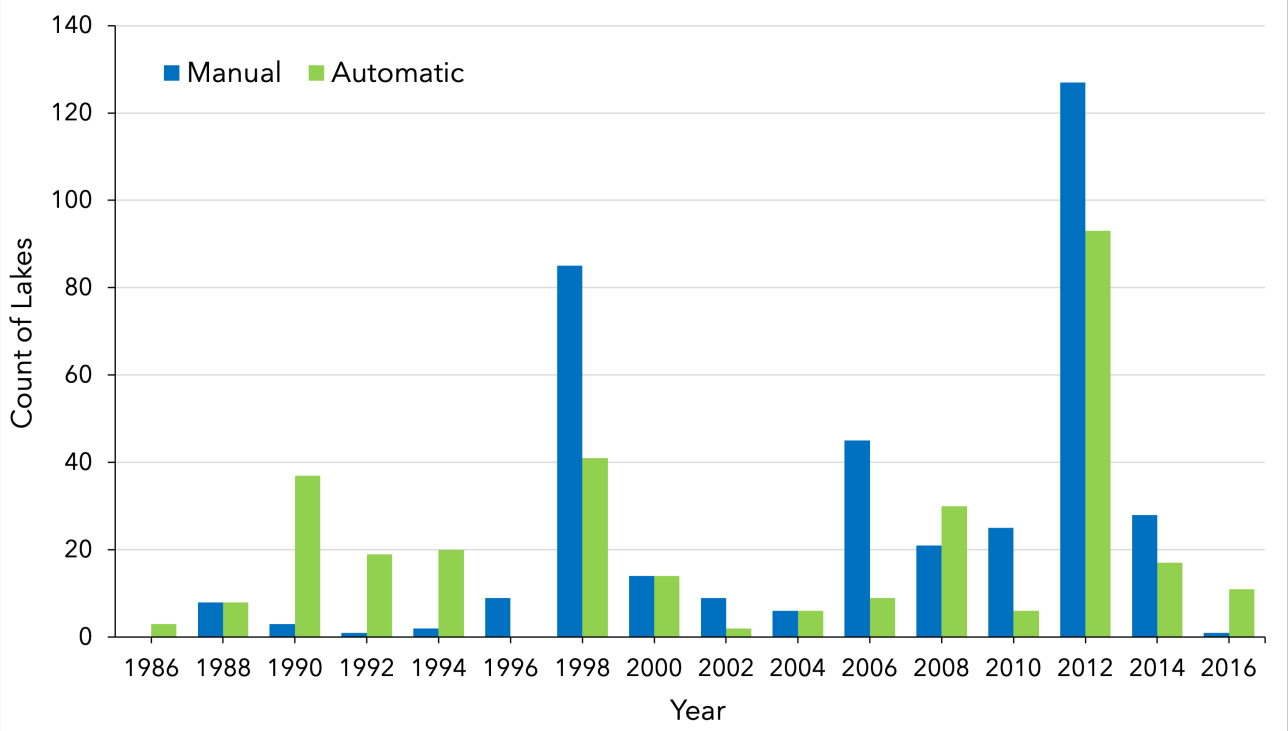

Figure 10. Comparison of manual (blue) and automatic (green) detection of year of change for changed waterbodies on Banks Island. 2018 and 2020 are excluded to match the Banks Island dataset from Lewkowicz et al (2019), which includes only up to 2016.

Despite these discrepancies, the automatic method is clearly a helpful and easily interpretable method for assigning a single year of greatest change to colour-changed waterbodies, in order to assess the temporal pattern of such change across Northern Canada.

5. Results

5.1 Spatial Analysis

5.1.1 Waterbody Colour Change Classification

The overall accuracy for the random forest classification was 91.8%, with an AUC score of 0.95. Changed waterbodies had a producer accuracy of 78.6%, a user accuracy of 94.2%, and an F1 score of 0.86, while unchanged waterbodies had a producer accuracy of 97.8%, a user accuracy of 90.9%, and an F1 score of 0.94. Generally, the accuracy results showed that the model performs well. There was a total of 333,084 waterbodies classified as changed and 1,120,380 waterbodies classified as unchanged. The changed waterbodies cover an area of 55,219 km^2, representing 17.3% of the total waterbody area

in the study region. Figure 11 shows the distribution of changed and unchanged waterbodies (>1 ha) by size, and Table 3 shows summary statistics for the changed and unchanged waterbodies.

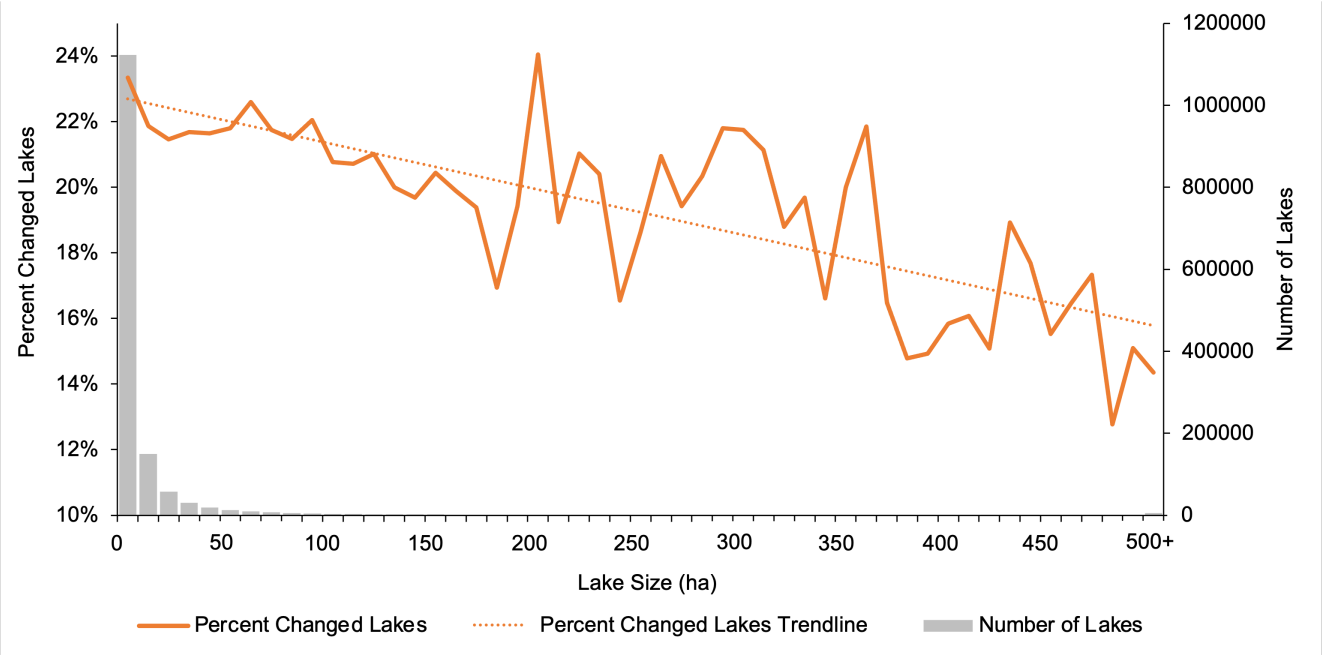

Figure 11. Percentage of changed lakes, with linear trendline (y= -0.0014x + 0.2283), and total number of lakes by waterbody size. 95% of waterbodies in the dataset are under 50 ha. 0.38% are over 500 ha (represented by the 500+ bin).

Table 3. Waterbody size statistics for changed and unchanged waterbodies.

	All Waterbodies	Changed Waterbodies	Unchanged Waterbodies
N (>1 ha)	1453464	333084 (22.9%)	1120380 (77.1%)
N (>500 ha)	5588	802 (14.4%)	4786 (85.6%)
Maximum (ha)	487502	487502	421848
Median (ha)	3.43	3.18	3.51
Total Area (km2)	318838	55219	(17.3%)

The proportion of changed to unchanged waterbodies across size profiles is higher in in Figure 11 and Table 3 show that there is a downward trend in percentage of changed waterbodies as waterbody size increases. This trend could be explained by the method in which reflectance was calculated for each waterbody and the possible mechanisms of change. Waterbody reflectance values were calculated based on the median of all water pixels in the waterbody thus descreasing the impact of small coastal change mechanisms on the waterbody's colour as a whole for larger waterbodies.

Table 4 shows the mean accuracy of the classification by area. The accuracy varied slightly across areas, ranging from 84.12% to 100% accuracy. These regional results indicate a stronger performance in regions with a higher proportion of unchanged waterbodies, owing to the greater accuracy of the classifier for the detection of unchanged waterbodies.

Table 4. Regional accuracy results for all training regions used to train the machine learning classification algorithm.

Sample Area	Count of Changed Waterbodies	Count of Unchanged Waterbodies	Mean Accuracy (10-fold Cross Validation)
Area1	0	102	100.00%
Area2	84	140	91.04%
Area3	69	136	86.26%
Area4	6	149	98.75%
Area5	3	124	97.69%
Area6	65	92	84.12%
Banks	256	323	96.03%

5.1.2 Spatial Pattern of Change

Figure 12 shows the result of the classification for all waterbodies in the study area. Areas with many waterbodies classified as changed are shown as bright yellow, while regions with many unchanged waterbodies are shown in blue. Figure 13 shows the spatial pattern of waterbody change across Northern Canada, with waterbodies aggregated into 10km x 10km grids based on the density of all waterbodies and the density of changed waterbodies in the study area. Light grey areas are regions with very few to no waterbodies. Bright green areas are regions with a low proportion of waterbody area relative to the total area of the grid (100km^2) but with a high proportion of changed waterbodies. Bright blue areas are the opposite: areas with a large proportion of waterbodies where a minority changed at some point in the time period (most waterbodies stayed the same). Purple areas are areas with a high proportion of waterbodies relative to the total area and a high proportion of those waterbodies experienced change.

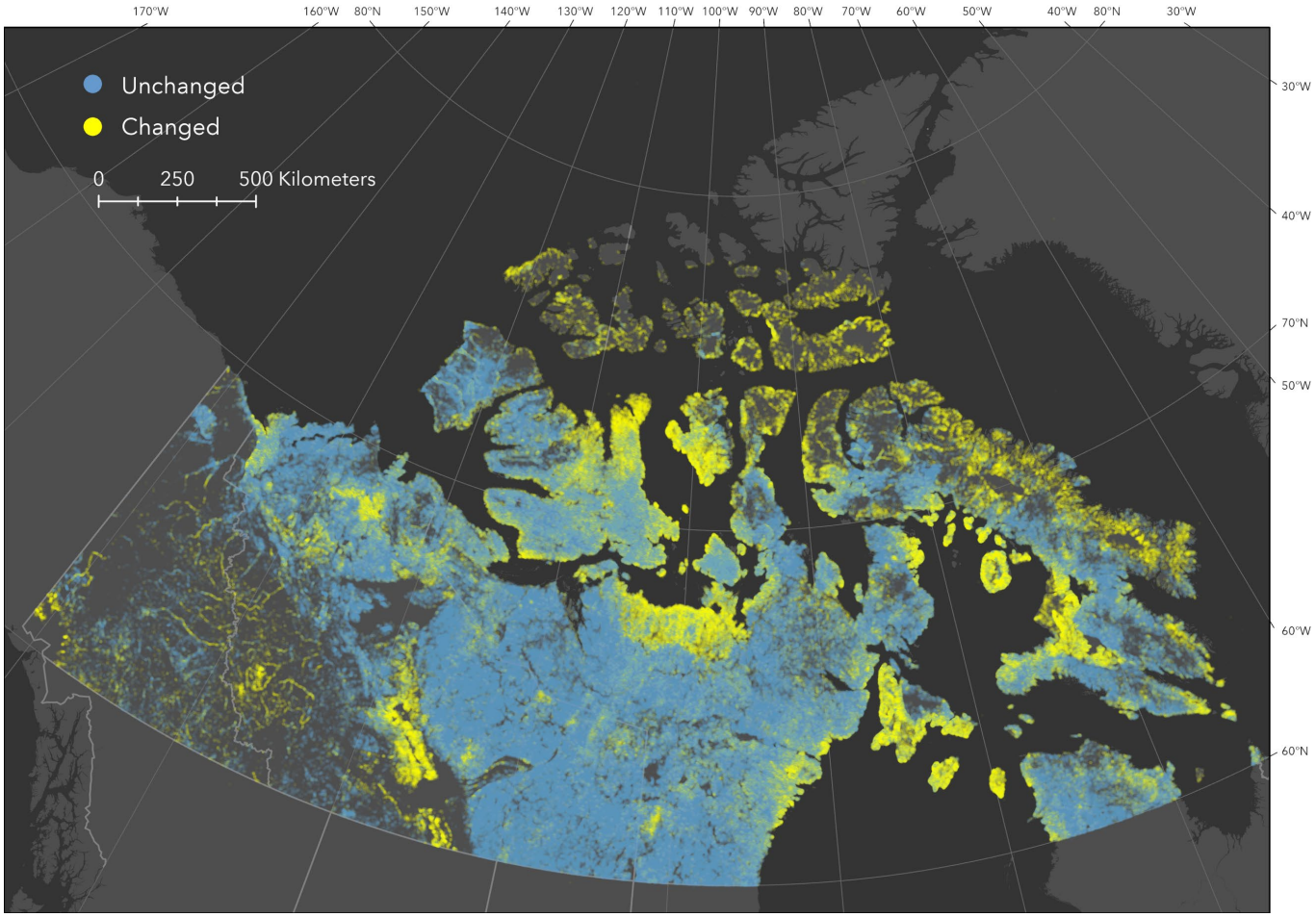

Figure 12. Changed and unchanged waterbodies across Northern Canada represented by their centroid points. Points are 95% transparent so regions with brighter colours indicate higher waterbody density. Legend symbols enlarged for clarity.

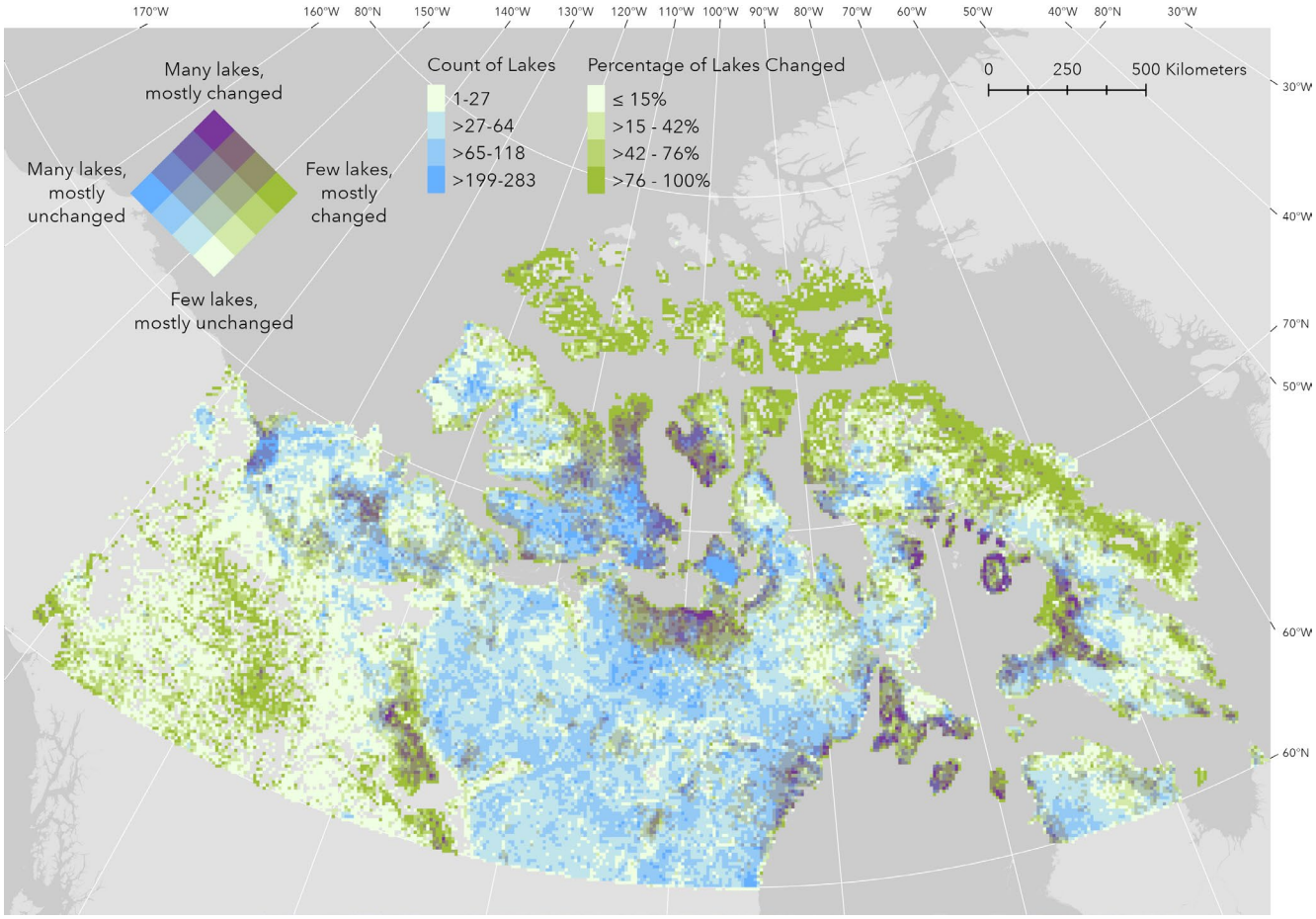

Figure 13. Spatial pattern of proportion of changed waterbodies relative to the total number of waterbodies from 1984-2021. Grids are 10km x 10km.

There is a clear spatial pattern in the distribution of changed waterbodies across the study area in Figure 12 and Figure 13. Most of the very high north (north of 74°N) has low waterbody density but a proportionally high density of changed waterbodies (shown in bright green in Figure 13). The regions with many changed waterbodies (shown as yellow in Figure 12 and as purple in Figure 13) mostly occur in coastal areas, with some prominent clusters on Victoria Island, the area south of the Queen Maud Gulf, and the region between Great Bear Lake and Great Slave Lake. Aside from those areas, the majority of waterbodies in the continental interior show little change (shown in bright blue in both figures).

Figure 14-Figure 17 show the classification results for some of the regions with many changed waterbodies, identified above. These sample images show that the classification was successful at identifying changed waterbody color in these regions. The waterbodies with clear visual change, going

from a dark clear blue colour to a turbid brown, are classified as changed, while adjacent waterbodies that stayed visually clear throughout the time period were classified as unchanged. There is some discrepancy between the classification and visual appearance of change in the imagery because waterbodies are classified as changed based on the entire time series of images while for clarity the figures are limited to images from two time periods.

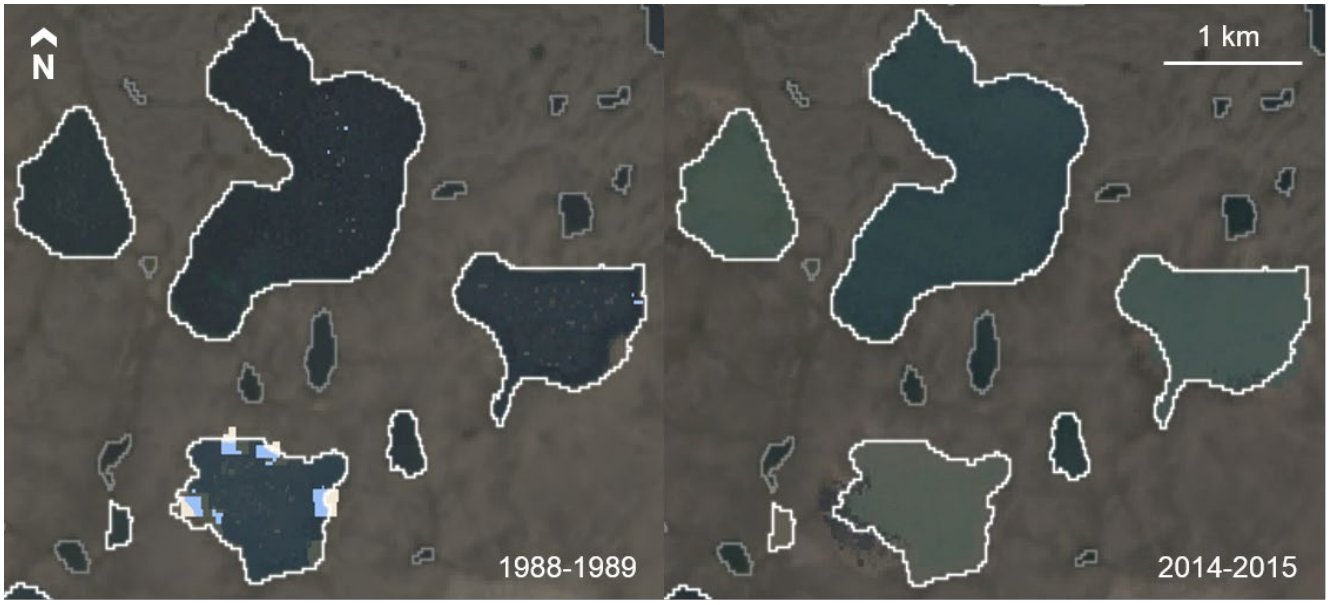

Figure 14. Comparison of waterbody colour and classification result near Bluenose Lake, NWT. Waterbodies classified as changed are outlined in white and waterbodies classified as unchanged are outlined in grey. Missing pixels show basemap. Lat: 68.599, Lon: -119.227. Note that change may have happened in other years than those shown here, so waterbodies classified as "changed" despite having similar appearance in 1988-89 and 2014-15 may still be correctly classified.

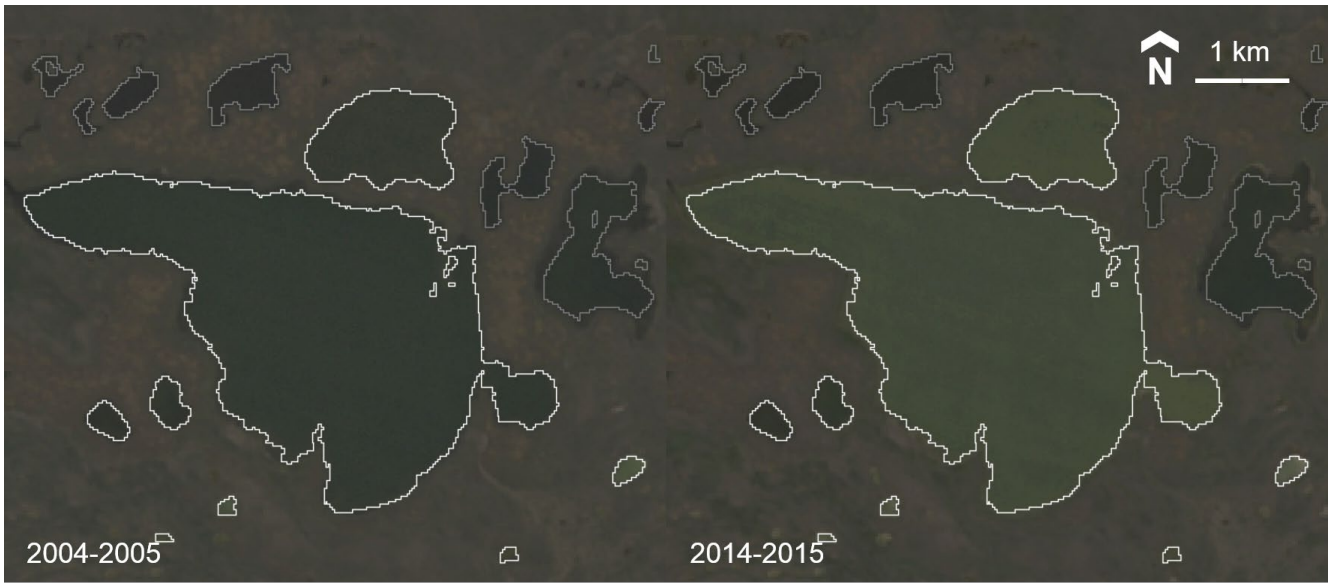

Figure 15. Comparison of waterbody colour and classification result near Lac Levis, NWT. Waterbodies classified as changed are outlined in white and waterbodies classified as unchanged are outlined in grey. Lat: 62.503, Lon: -117.700.

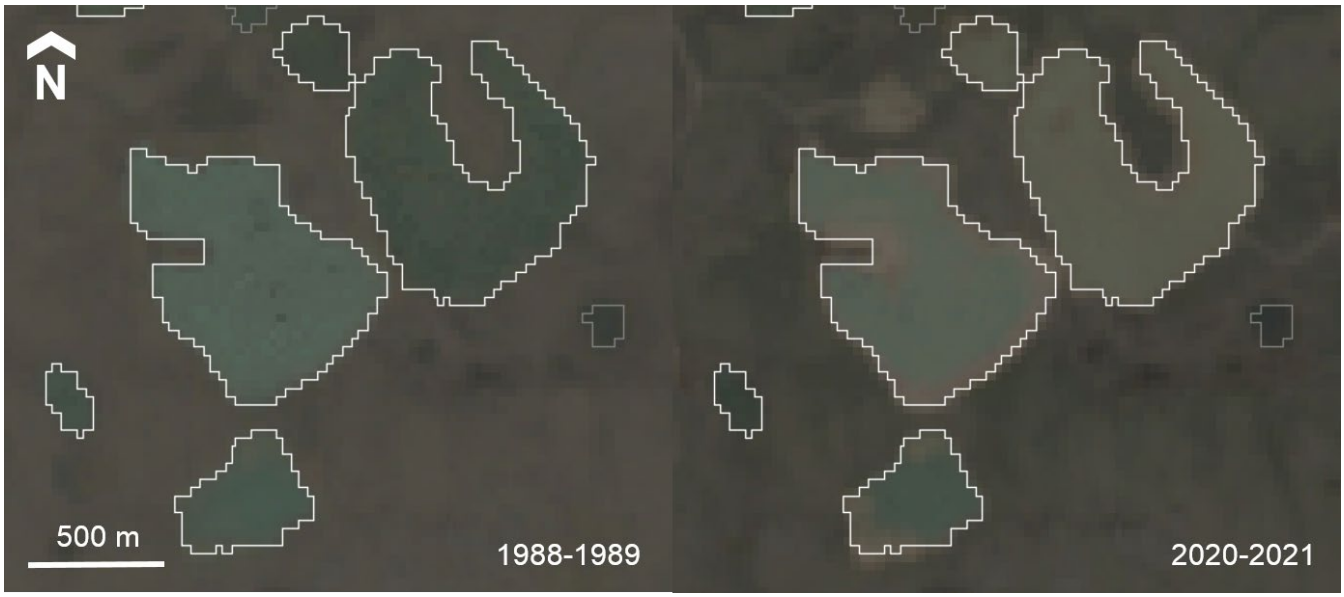

Figure 16. Comparison of waterbody colour and classification result near Queen Maud Gulf Bird Sanctuary, Nunavut. Waterbodies classified as changed are outlined in white and waterbodies classified as unchanged are outlined in grey. Lat: 67.587, Lon: -97.790

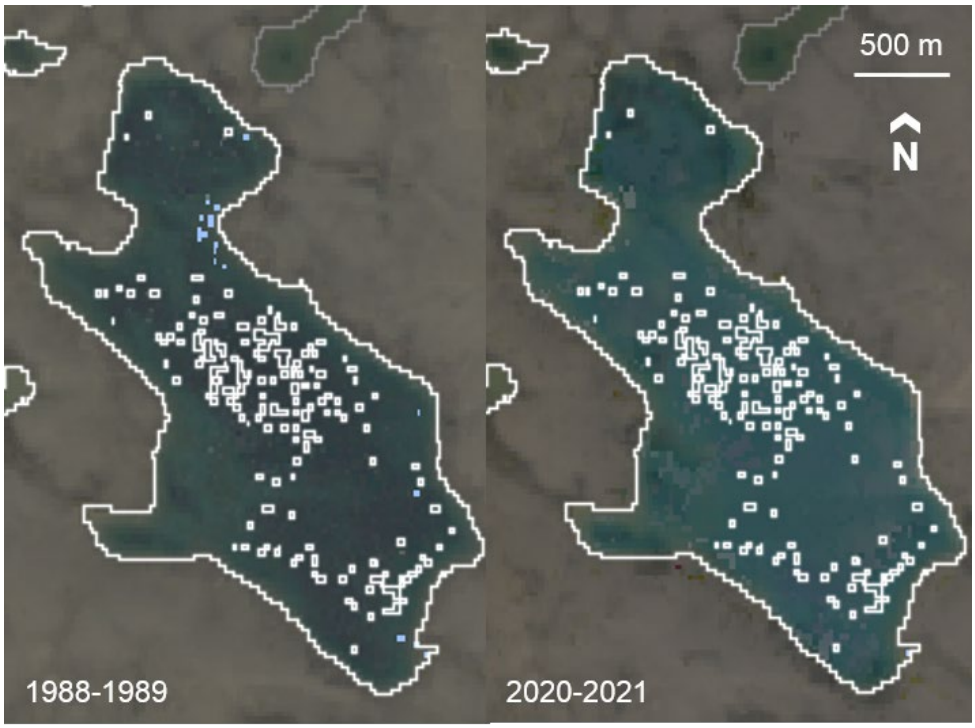

Figure 17. Comparison of waterbody colour and classification result on the north-eastern section of Victoria Island. Waterbodies classified as changed are outlined in white and waterbodies classified as unchanged are outlined in grey. Pixelated region indicates that some interior pixels were excluded from the waterbody extent. Lat: 72.442, Lon: -106.378

5.2 Temporal Analysis

5.2.1 Temporal Patterns of Change

Figure 18 shows the distribution of maximum year of change for all changed waterbodies with (a) and without (b) the inclusion of the year 1992. The mosaic for 1992-1993 was brighter overall than 1994-1995, resulting in a false peak of 'change' (Figure 18 a) so it was removed from the analysis (Figure 18 b) to more appropriately distribute the year of maximum change for each waterbody. However, by removing 1992 from this portion of the analysis, we also lose the ability to identify waterbodies that did actually show real change in 1992 and uses instead the year of second largest change for those waterbodies.

The early years show considerably more change than later years, which is possibly influenced by increased variation in the quality of the mosaic imagery due to fewer available images (Figure 6). However the pattern in later years clearly shows some years with comparatively more change, including 2008, 2012, and 2020, while the mosaic quality across those later years is consistent.

Figure 19 shows the temporal pattern of the year of greatest change in the green band for all changed waterbodies. Waterbodies are represented by their centroids and set to 80% transparency in order to show the pattern in regions of high waterbody density. 1986 was excluded to reduce the impact of missing pixels in early years (see Figure 6)

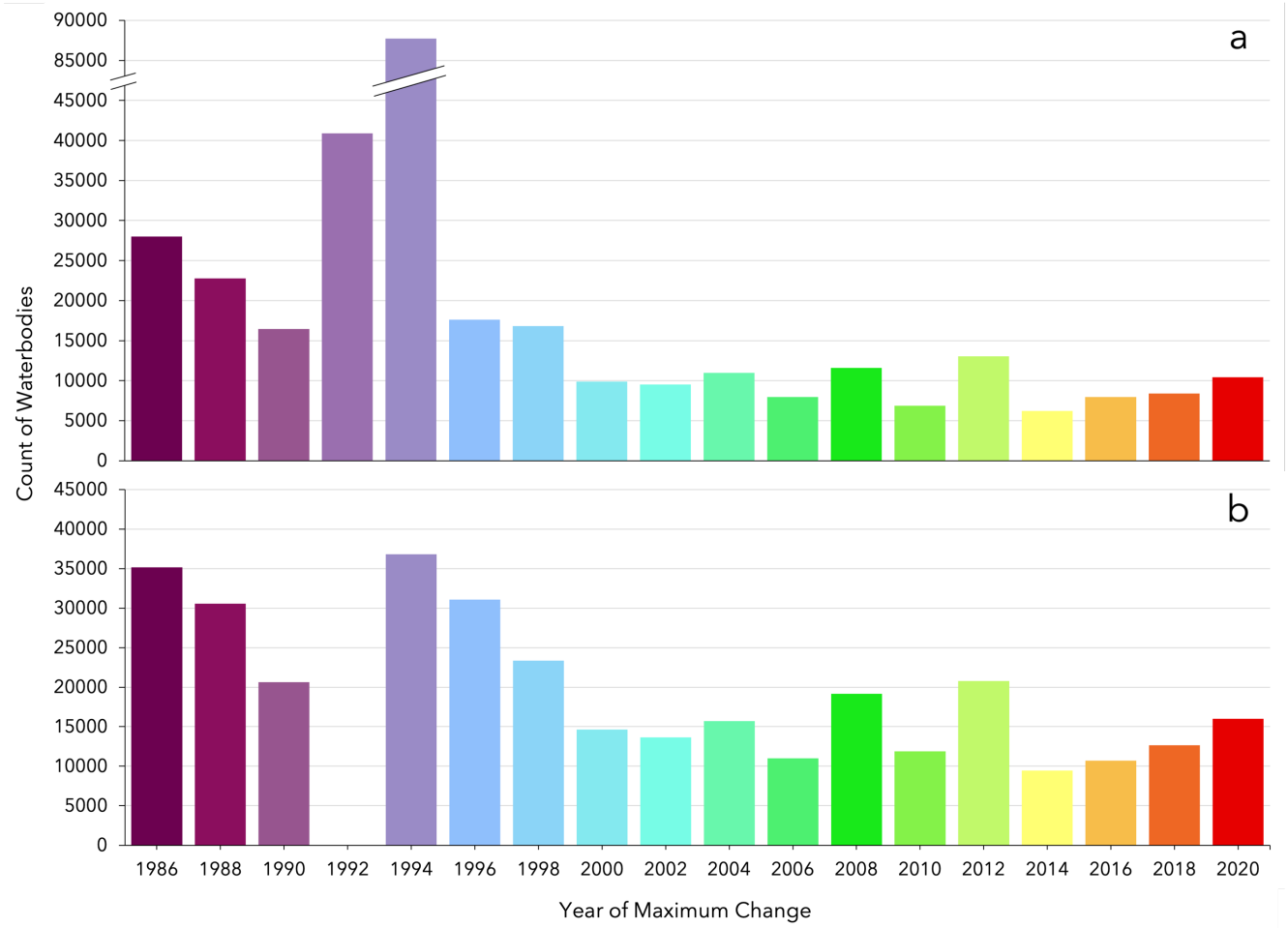

Figure 18. Maximum year of change in the green band for all changed waterbodies (a) including all annual values and (b) excluding 1992-1993 prior to differencing. The year shown on the x-axis represents the beginning of the later of the two periods used to calculate the difference, e.g. 2020 indicates that the greatest difference in reflectance values happened between 2018-2019 and 2020-2021. In b, 1994 indicates the difference between the mosaic values for 1990-1991 and 1994-1995.

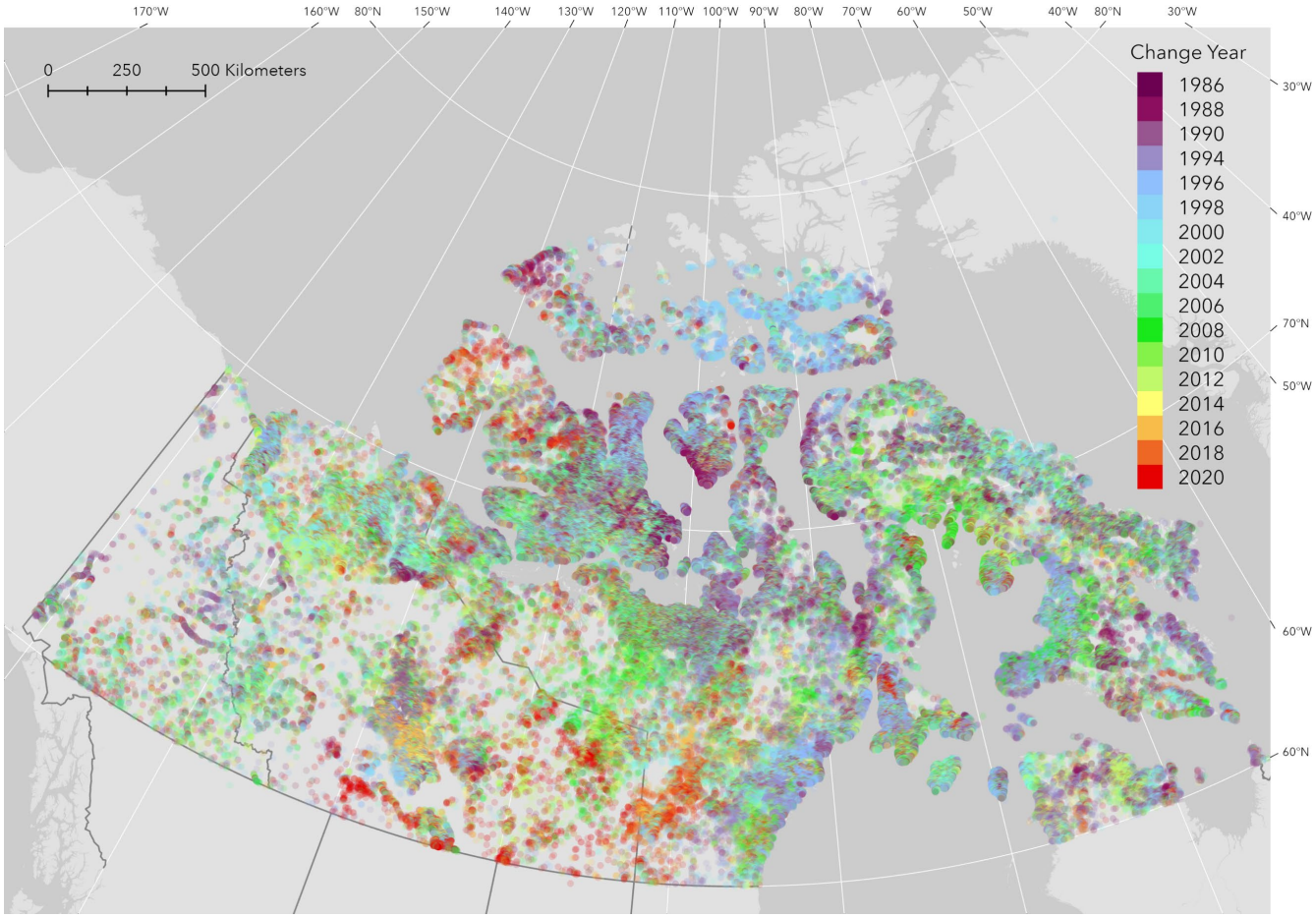

Figure 19. Maximum year of change in the green band for all changed waterbodies. The year represents the later of the two years used to calculate the difference, e.g. 2020 indicates that the greatest difference in reflectance values for a particular waterbody was between 2018 and 2020.

The pattern of temporal change (Figure 19) shows high variability across the entire study area. However, there are regions of clear spatial clustering of change timing. There are several clusters of orange to red colours at lower latitudes, indicating later colour change, in the central southern portion of the study area of Figure 18, as well as around Banks Island and the western coast of Victoria Island. There are also apparent clusters of early change in the 1990s (purple) and mid-2000s (green) spread out across Northern Canada with no broader-scale pattern. The region south of Queen Maud Gulf around the Queen Maud Gulf Bird Sanctuary (QMG) has a high density of waterbodies and appears to have a gradient from west to east of primarily green (changes in the mid 2000s) to primarily purple (changes in the late 1980s). Another region with high density is the area between Great Slave Lake and Great Bear Lake (GSGBL) where there is a cluster of orange (2016) change. Time series of these regions show that both the QMG and GSGBL regions experience frequent ongoing change. The

distribution of years of change does not show a general temporal gradient from low to high latitudes. The spatial distribution of maximum year of change thus appears to be influenced primarily by local processes or environmental conditions.

Figure 20 compares the timing of greatest waterbody colour change with the mean July-August air temperature for the same area, for the entire area between 60°N and 74°N in orange, Banks Island in blue, and the QMG region in red. The temperature trend for all three areas shows regional differences in the early half of the study period but follow the same general trend in the latter half of the time period, with warm peaks around 2010-2012 and 2016, and colder temperatures around 2014 and 2018. The pattern of timing of greatest waterbody colour change is distinct across the three areas. The area between 60-74°N has a strong peak in 1994, while the other areas show significant change in early years (QMG) and late years (Banks Island).

The comparison with temperature shows some possible connection, particularly for Banks Island, where peaks of colour change timing appear to coincide with relatively high summer temperatures for 1994, 1998, and 2012. However, temperature does not appear to be the sole factor, as peaks in change timing are not always associated with temperature peaks, as in 2018 and 2020 for Banks Island, and 2006 for the red region. While temperature has a well-studied impact on permafrost thaw and thus water colour change, this relationship is complex and not obvious from the direct comparison of temperature and change timing in Figure 20.

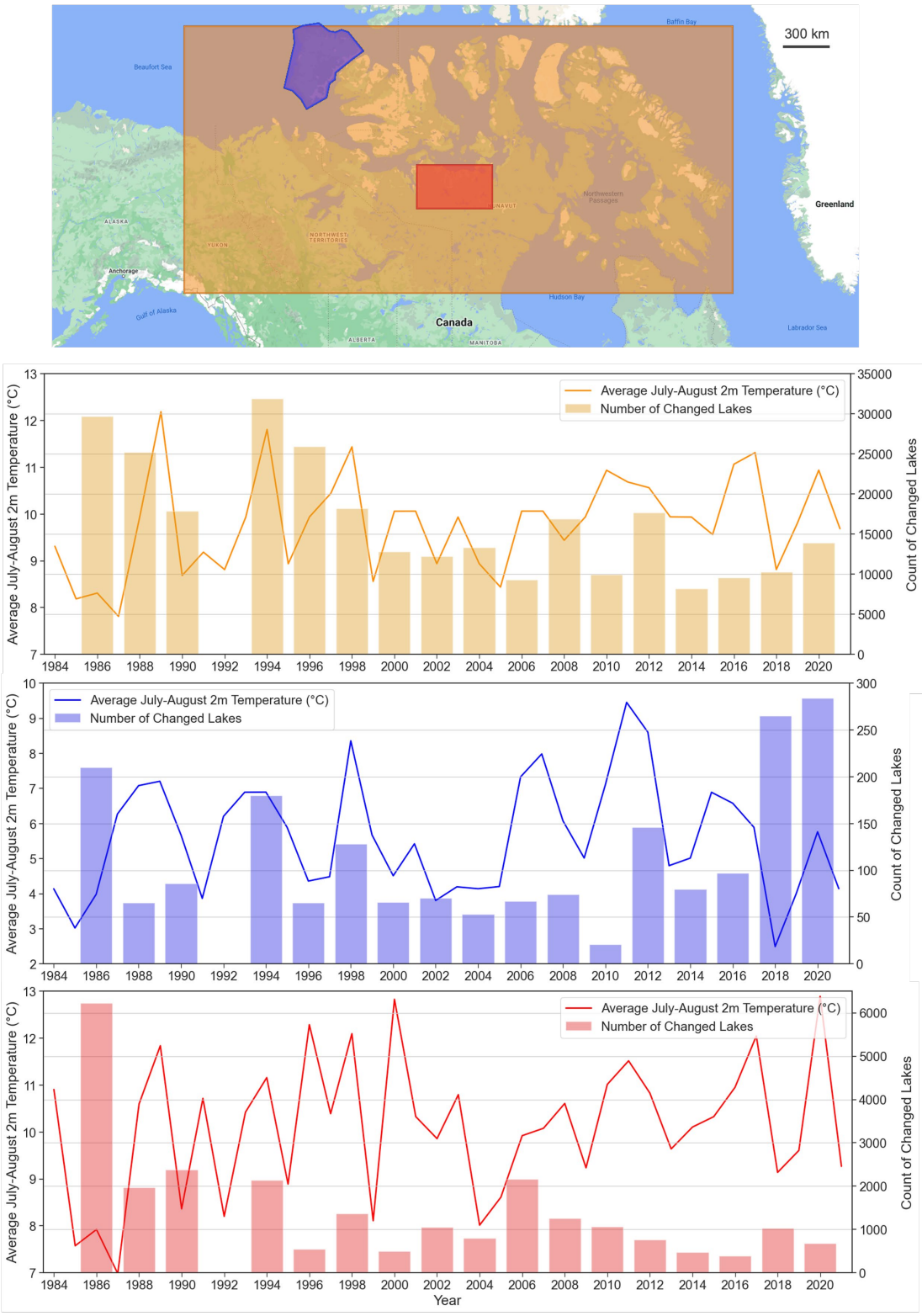

Figure 20. Mean July-August temperature and biennial waterbody change counts comparison. Monthly-mean temperature (2m) averages retrieved from ERA5-Land dataset post-processed by ECMWF. Both temperature data (average) and count of changed waterbodies by year of change (sum) were summarized for each region shown on the map (all of northern Canada between 60N and 74N in orange, Banks Island in blue, and the region south of the Queen Maud Gulf (QMG) in red) in Google Earth Engine.

6. Discussion

Long time series of high-resolution satellite imagery are essential for monitoring dynamic inland water quality changes. The enormous quantity of freely available Landsat data is an exceptional source of data for investigating water quality change across large timescales, but data processing can be very intensive. Cloud computing resources such as Google Earth Engine allows users to process large amounts of data quickly and efficiently, allowing for the development of methodologies to detect spatial and temporal patterns across large areas and long time periods with relative ease. Google Earth Engine and Landsat data have been widely used for studies quantifying landcover change and waterbody dynamics across a large spatial scope (Deines et al., 2019; Dong et al., 2016; Duan et al., 2020; Fu et al., 2022; Guo et al., 2022; Huang et al., 2017; Noi Phan et al., 2020; Wang et al., 2022; Zhou et al., 2019). In this study, we used Landsat data and the processing power of Google Earth Engine to assess inland waterbody colour change between 1984 and 2021 across Northern Canada. Across this period, we found that 22.9% of all waterbodies in Northern Canada underwent visually obvious colour change, and we outlined previously unknown spatial and temporal patterns of such change.

6.1 Spatial Patterns of Change

This study is the first to assess the spatial pattern of inland waterbody colour change across Northern Canada. We found strong spatial clustering of colour change, with changes primarily happening along coastlines, and with larger clusters of change occurring farther inland on northern Victoria Island, along the southern coast of the Queen Maud Gulf (QMG) and between Great Slave Lake and Great Bear Lake (GSGBL).

These clusters of water colour change do not share permafrost or physiographic characteristics. They are spread across areas with continuous and extensive discontinuous permafrost, and have varying levels of ground ice content; Victoria Island lies within a zone of high ground ice content while the QMG and GSGBL regions are within zones with low ground ice content. The clusters are also spread across several physiographic regions including the Interior Plains, Arctic Lowlands and the Canadian Shield.

The variety in landscape characteristics across areas with high levels of waterbody colour change suggests diversity in the mechanisms and types of changes occurring in these regions. This is supported by the variance we see in the time series of reflectance values for individual waterbodies in these regions. In regions like Banks Island and Victoria Island, where water colour change has previously been correlated with above-average temperatures and adjacent permafrost activity, waterbody colour change is usually abrupt, happening over the course of 1-2 years. These waterbodies generally experience just one instance of colour change throughout the 1984-2021 period, typically from clear blue to turquoise, but some undergo colour change multiple times. In other regions, including the QMG and GSGBL regions, the colour change is near-constant throughout the time series. These areas have high interannual variability in water colour, and fluctuate between bright and dark, often on a year-to-year basis. Unlike Banks Island, the mechanisms of change in these areas are less clear and could be the result of permafrost thaw processes or other factors entirely.

The overall accuracy of the random forest classification of changed and unchanged waterbodies is good, but there is some variation in how well it identified changed vs. unchanged waterbodies. True changed waterbodies are more often misclassified than true unchanged waterbodies (changed producer accuracy of 78.6% vs. unchanged producer accuracy of 97.8%). As a result, this study likely underestimates the true number of changed waterbodies. However, these findings may be regionally biased by the locations of the areas used to train, validate and test the model. These areas were geographically distributed among the waterbody-rich regions of the study area, but with Banks Island (northernmost point around 74°N) as the northernmost location used for training the model, the sparse waterbodies north of Banks Island in the Arctic Archipelago were not represented in the training data. Visual inspection of the classification result and biennial imagery for these very high latitude waterbodies suggests ice contamination in the images could have led to misclassification of unchanged (but regularly ice-covered) waterbodies. Consequently, the classification results for the Queen Elizabeth Islands of the Canadian Arctic Archipelago, the cluster of islands north of 74.5°N, should be interpreted carefully and with lower confidence.

This points to room for improvement in two areas: the compositing method and the masking of ice. In this study, we used a composite pixel method and opted to use a darker-than-median pixel in order to minimize ice contamination in the image mosaics. The 25^{th} percentile was chosen because it generally

worked well across the entire area, however the inclusion of abnormally bright pixels in the mosaics did still occur occasionally. Given the variety of environment types across Northern Canada and the steep gradient in temperature between the lower latitudes of Northern Canada (60°N) and the glaciated northern tips of the Arctic Archipelago, a one-size-fits-all method may not be the best way to mosaic imagery in Northern Canada. The compositing method used in this study is useful for comparing imagery objectively between different locations, and thus assessing trends across large areas, but more localized or geographically varying compositing methods may be more useful for assessing trends within particular areas of interest. Future studies may find more success in applying a more regional approach to compositing, based on the ice-free season of a particular area and the range of reflectances that are considered normal in those regions.

Alternatively, improvements in masking out thin layers of ice and snow may also improve the performance of large-scale studies. In colder locations, waterbody ice-cover sometimes stays year-round and if those pixels are not properly masked out, the variance between dark pixels with no ice and bright pixels with some ice cover can be mistaken as colour change. This study used CFmask to eliminate cloud- and ice-contaminated pixels; this is an often-used method, despite variable performance. Improved methodologies for masking out snow and ice, particularly thin layers of ice overtop waterbodies, would reduce image contamination by icy pixels and avoid misclassification. The incorporation of radar data for snow and ice masking in particular could be very useful for higher latitudes with shorter or rarer ice-free seasons.

This study considers colour change as a binary process—it is either happening or it is not—but in reality water colour change is a dynamic and often gradual process, linked to a waterbody's hydrological and ecological processes and constantly undergoing change. Despite the continuous nature of waterbody colour change and the subjectivity of coercing continuous data into categories of changed or unchanged, it is useful to apply a threshold to distinguish substantial and meaningful change from the minute changes in colour all water bodies experience on a daily basis, identify trends in the data on waterbody colour, and link those trends back to the underlying mechanisms of change. This study thus categorizes waterbodies as changed or unchanged to identify the spatial and temporal patterns of significant colour change. Now that change has been identified in these areas, future studies

can further examine the nature and mechanisms of change and how they relate back to physical processes in the waterbody and surrounding landscape.

The Mann-Kendall test and Theil-Sen slope are widely used for trend analysis in remote sensing (Militino et al., 2020; Thakur et al., 2021) however, they are both primarily used for detecting linear trends; the Mann-Kendall test specifically looks for monotonic trends while the Theil-Sen slope provides a linear slope through the points of data. This makes them well suited for detecting change that occurs consistently in one direction, e.g. when a waterbody becomes increasingly or decreasingly reflective over time. However, these metrics may be poor indicators of pulsed or continuous change that both increases and decreases a waterbody's reflectance over time, as when turbidity is constantly fluctuating. The results of this study show that despite this potential limitation, the accuracy of the classifier is still high for the continuously changing waterbodies in the QMG and GSGBL regions.

6.2 Temporal Patterns of Change

This study used the single year of greatest reflectance change in the green band to assess the temporal pattern of waterbody colour change across northern Canada with some success. This method corresponds well with the timing of waterbody colour change on Banks Island where the change generally occurs just once and is abrupt, with colour changing substantially from one year to the next. However, this method assumes that waterbodies change colour just once and that the brightness levels across mosaics are consistent, neither of which are always true.

Identifying single years of change is useful in regions with abrupt distinctive change because it can be used to relate the change to environmental factors that may be implicated in the physical processes causing it. By contrast, identifying a single year of change is less useful when change is frequent or continuous and slow, evolving over the course of many years. In those cases, identifying the single year of greatest change could be useful and highlight a year of significant change across many waterbodies, but it could also distract from the understanding of colour change as a continuous process.

The brightness levels across the biennial image mosaics must be consistent for detected changes in this brightness to correspond to environmental changes in the water. The use of a single percentile (in this

case the 25th percentile) to create the composite imagery assumes that the distribution of pixel brightness is consistent from year to year, and specifically that the 25th percentile allows the composite imagery to exclude pixels contaminated by clouds, ice and snow (bright) as well as cloud shadow (dark) and reflect the typical water colour of the two-year period. This is a safe assumption when the sample size is large, as when there are many ice-free and cloud-free images over the two years from which pixels are sampled for the composites, but abnormal conditions, which are likely in years with few available images, can bias the overall brightness of the mosaic to be darker or lighter than normal. In these cases, a waterbody may not have changed colour from the previous period, but the compositing method may be unable to accurately reflect typical water colour across the image mosaic, leading to errors in the detection of change, including its timing. This is particularly challenging when trying to identify real change in the early years of the study period, when the image mosaics had many fewer usable pixels (Figure 6).

Furthermore, it is difficult to assess the accuracy of the automatic method of detecting year of chang using the maximum magnitude of interannual reflectance change. Although the human eye is good at detecting colour change between images, as was done to train and test the model, it is not very good at assessing the magnitude of change relative to other changes, especially if these changes are dissilmilar in nature (e.g. from dark blue to brown, vs. dark blue to green), as is necessary to determine the year of greatest change. In this study, the distribution of the year of greatest change (i.e. one year of greatest change per waterbody) was compared to the distribution of all detected years of change (i.e. greater than or equal to one change per waterbody). This showed some congruency between the two, with spikes occurring at similar times for both the visual detection of each waterbody change and the automatic detection of a single change, but works best when there are few colour changes happening to a waterbody over the course of the time series.

Given the known relationship between waterbody colour change and permafrost thaw activity, temperature is the most likely contributor to waterbody colour change. However, Figure 19 showed no clear relationship between the timing of colour change and the temperature signal for a given area. This could be due to a lag between high temperatures and subsequent permafrost activity contributing to water colour change, which makes a direct interpretation of Figure 19 difficult. Additionally, the best reason to believe that temperature is a factor in waterbody colour change is when increased

temperatures lead to permafrost thaw activity and thus higher turbidity. This mechanism would only be reflected in changes where brightness increases. However, the year of change in this study is determined by an absolute change in brightness, i.e. the waterbody could have increased or decreased in brightness in that time, leading to further complexities when interpreting the relationship between colour change and temperature. Overall, Figure 19 suggests that while temperature is important, its relationship to colour change is complex and is likely just one of many contributing factors to water colour change.

6.3 Limitations

This study demonstrates that water colour change can be successfully detected automatically across a very large area, however, the method of using visual detection of colour change to train a model does not provide insight into the physical processes causing this change to happen in a given area. Of the colour change indicators used to train the classifier, only turbidity is a metric of waterbody constituents, the rest are simple surface reflectances in the visible bands. This study was limited by a lack of in-situ water quality data for waterbodies in Northern Canada, which would be needed to calibrate algorithms to quantify other physical water quality metrics such as Secchi disk depth, chlorophyll concentration, total suspended solids, and coloured dissolved organic matter. Other than turbidity, at the time of analysis the published methodologies for detecting those waterbody constituents across the large spatial scope of this study require calibration with local in-situ data. It would be ideal to have in-situ training data for water quality to improve the interpretation of this type of automatic detection and attribute colour change to a specific type of change in water quality, which is more closely linked to the physical processes underlying change than the colour change itself. The collection of water quality data for these purposes would be labour intensive and points to the need for more open-source collaboration and sharing platforms for Northern water quality data, akin to Lake Pulse in southern Canada and Aquasat in the United States (Huot et al., 2019; Ross et al., 2019).

7. Conclusion

This study used a machine learning method to classify waterbodies across Northern Canada as colour-changed or unchanged since 1984 from cloud- and ice-free Landsat TM, ETM+ and OLI biennial pixel composite mosaics created with Google Earth Engine. In total, this study assessed the colour trend in

over 1.4 million waterbodies across the 4 million square kilometer study area and found over 330,000 waterbodies (22.9%) to have changed colour over the period 1984 to 2021. The use of pixel composite mosaics, as opposed to individual images, allowed us to maximize the usable data from the entire Landsat collection and use a single methodology for assessing colour change across the large spatial extent of the study area.

Results show strong spatial clustering of change, particularly in coastal areas and in certain inland areas such as the plain between Great Bear Lake and Great Slave Lake. Areas with many waterbodies undergoing or having undergone change are geographically diverse, both in terms of their location and their permafrost and substrate conditions. The types of colour change were likewise diverse across these areas, with some waterbodies undergoing simple and obvious change from one year to the next, and others undergoing gradual or continuous change across an extended time period. These findings indicate that the processes driving waterbody colour change are likely dependent on diverse local factors.

As waterbody dynamics are important indicators of change in northern landscapes, these findings will help to improve monitoring efforts and increase understanding of the spatial and temporal patterns in the landscape's response to a rapidly warming northern environment. By identifying clusters of significant waterbody colour change across Northern Canada, this study contributes important information for the basis of future studies on the local patterns and mechanisms contributing to water colour change and other climate-change driven impacts in those regions. The code for this project will be made publicly available for transparency and to provide a base framework for future large-scale water quality monitoring projects.

8. References

Aas, E. (1996). Refractive index of phytoplankton derived from its metabolite composition. *Journal of Plankton Research*, *18*(12). https://doi.org/10.1093/plankt/18.12.2223

Abdelrhman, M. A. (2017). Quantifying Contributions to Light Attenuation in Estuaries and Coastal Embayments: Application to Narragansett Bay, Rhode Island. *Estuaries and Coasts*, *40*, 994–1012. https://doi.org/10.1007/s12237-016-0206-x

Anthony, K., Schneider von Deimling, T., Nitze, I., Frolking, S., Emond, A., Daanen, R., Anthony, P., Lindgren, P., Jones, B., & Grosse, G. (2018). 21st-century modeled permafrost carbon emissions accelerated by abrupt thaw beneath lakes. *Nature Communications*, *9*(1). https://doi.org/10.1038/s41467-018-05738-9

Berteaux, D., Reale, D., McAdam, A. G., & Boutin, S. (2004). Keeping Pace with Fast Climate Change: Can Arctic Life Count on Evolution? *Integrative and Comparative Biology*, *44*(2), 140–151. https://doi.org/10.1093/icb/44.2.140

Bouchard, F., Francus, P., Pienitz, R., Laurion, I., & Feyte, S. (2014). Subarctic Thermokarst Ponds: Investigating Recent Landscape Evolution and Sediment Dynamics in Thawed Permafrost of Northern Québec (Canada). *Arctic, Antarctic, and Alpine Research*, *46*(1), 251–271. https://doi.org/10.1657/1938-4246-46.1.251

Bowers, D. G., Braithwaite, K. M., Nimmo-Smith, W. A. M., & Graham, G. W. (2009). Light scattering by particles suspended in the sea: The role of particle size and density. *Continental Shelf Research*, *29*(14). https://doi.org/10.1016/j.csr.2009.06.004

Bratby, J. (2014). Turbidity: Measurement of Filtrate and Supernatant Quality? In *Progress in Filtration and Separation*. https://doi.org/10.1016/B978-0-12-384746-1.00016-1

Breiman, L. (2001). Random Forests. *Machine Learning 2001 45:1*, *45*(1), 5–32. https://doi.org/10.1023/A:1010933404324

Brezonik, P., Menken, K. D., & Bauer, M. (2005). Landsat-based remote sensing of lake water quality characteristics, including chlorophyll and colored dissolved organic matter (CDOM). *Lake and Reservoir Management*. https://doi.org/10.1080/07438140509354442

Brothers, S., Kö Hler, J., Attermeyer, K., Grossart, H. P., Mehner, T., Meyer, N., Scharnweber, K., & Hilt, S. (2014). A feedback loop links brownification and anoxia in a temperate, shallow lake. *Limnology and Oceanography*, *59*(4), 1388–1398. https://doi.org/10.4319/lo.2014.59.4.1388

Brown, J., Ferrians, O., Heginbottom, J. A., & Melnikov, E. (2002). *Circum-Arctic Map of Permafrost and Ground-Ice Conditions, Version 2*. https://doi.org/https://doi.org/10.7265/skbg-kf16

Camill, P. (2005). Permafrost thaw accelerates in boreal peatlands during late-20th century climate warming. *Climatic Change*, *68*, 135–152.

Canadian Polar Commission. (2015). *State of Environmental Monitoring in Northern Canada*. http://arcticobservingcanada.ca/CPC_StateOfEnv_Eng_v1.10.pdf

Colombo, M., Brown, K. A., De Vera, J., Bergquist, B. A., & Orians, K. J. (2019). Trace metal geochemistry of remote rivers in the Canadian Arctic Archipelago. *Chemical Geology*, *525*, 479–491. https://doi.org/10.1016/J.CHEMGEO.2019.08.006

Comte, J., Monier, A., Crevecoeur, S., Lovejoy, C., & Vincent, W. F. (2016). Microbial biogeography of permafrost thaw ponds across the changing northern landscape. *Ecography*. https://doi.org/10.1111/ecog.01667

Dall'Olmo, G., Westberry, T. K., Behrenfeld, M. J., Boss, E., & Slade, W. H. (2009). Significant contribution of large particles to optical backscattering in the open ocean. *Biogeosciences*, *6*(6). https://doi.org/10.5194/bg-6-947-2009

De Beurs, K. M., & Henebry, G. M. (2004). Trend analysis of the pathfinder AVHRR land (PAL) NDVI data for the deserts of central Asia. *IEEE Geoscience and Remote Sensing Letters*, *1*(4). https://doi.org/10.1109/LGRS.2004.834805

Deines, J. M., Kendall, A. D., Crowley, M. A., Rapp, J., Cardille, J. A., & Hyndman, D. W. (2019). Mapping three decades of annual irrigation across the US High Plains Aquifer using Landsat and Google Earth Engine. *Remote Sensing of Environment*, *233*, 111400. https://doi.org/10.1016/J.RSE.2019.111400

Deshpande, B. N., Macintyre, S., Matveev, A., & Vincent, W. F. (2015). Oxygen dynamics in permafrost thaw lakes: Anaerobic bioreactors in the Canadian subarctic. *Limnology and Oceanography*. https://doi.org/10.1002/lno.10126

Deutsch, E. S., Fortin, M. J., & Cardille, J. A. (2022). Assessing the current water clarity status of ~100,000 lakes across southern Canada: A remote sensing approach. *Science of the Total Environment*, *826*. https://doi.org/10.1016/J.SCITOTENV.2022.153971

Dogliotti, A. I., Ruddick, K. G., Nechad, B., Doxaran, D., & Knaeps, E. (2015). A single algorithm to retrieve turbidity from remotely-sensed data in all coastal and estuarine waters. *Remote Sensing of Environment*, *156*, 157–168. https://doi.org/10.1016/j.rse.2014.09.020

Dong, J., Xiao, X., Menarguez, M. A., Zhang, G., Qin, Y.,

Thau, D., Biradar, C., & Moore, B. (2016). Mapping paddy rice planting area in northeastern Asia with Landsat 8 images, phenology-based algorithm and Google Earth Engine. *Remote Sensing of Environment*, *185*, 142–154. https://doi.org/10.1016/J.RSE.2016.02.016

Duan, Y., Li, X., Zhang, L., Liu, W., Liu, S. ', Chen, D., & Ji, H. (2020). Detecting spatiotemporal changes of large-scale aquaculture ponds regions over 1988-2018 in Jiangsu Province, China using Google Earth Engine. *Ocean and Coastal Management*, *188*, 105144. https://doi.org/10.1016/j.ocecoaman.2020.105144

Duguay, C. R., Zhang, T., Leverington, D. W., & Romanovsky, V. E. (2005). Satellite remote sensing of permafrost and seasonally frozen ground. In *Geophysical Monograph Series* (Vol. 163). https://doi.org/10.1029/163GM06

Dvornikov, Y., Leibman, M., Heim, B., Bartsch, A., Herzschuh, U., Skorospekhova, T., Fedorova, I., Khomutov, A., Widhalm, B., Gubarkov, A., & Rößler, S. (2018). Terrestrial CDOM in lakes of Yamal Peninsula: Connection to lake and lake catchment properties. *Remote Sensing*. https://doi.org/10.3390/rs10020167

Environment Canada. (2022). *Canadian Climate Normals (1981-2010)*. Environment Canada. https://climate.weather.gc.ca/climate_normals/index_e.html

Erasmi, S., Schucknecht, A., Barbosa, M. P., & Matschullat, J. (2014). Vegetation greenness in northeastern brazil and its relation to ENSO warm events. *Remote Sensing*, *6*(4). https://doi.org/10.3390/rs6043041

Fichot, C. G., Kaiser, K., Hooker, S. B., Amon, R. M. W., Babin, M., Bélanger, S., Walker, S. A., & Benner, R. (2013). Pan-Arctic distributions of continental runoff in the Arctic Ocean. *Scientific Reports*, *3*. https://doi.org/10.1038/srep01053

Finstad, A. G., & Hein, C. L. (2012). Migrate or stay: terrestrial primary productivity and climate drive anadromy in Arctic char. *Global Change Biology*, *18*(8), 2487–2497. https://doi.org/10.1111/j.1365-2486.2012.02717.x

Flood, N. (2013). Seasonal Composite Landsat TM/ETM+ Images Using the Medoid (a Multi-Dimensional Median). *Remote Sensing*, *5*(12), 6481–6500. https://doi.org/10.3390/rs5126481

Foga, S., Scaramuzza, P. L., Guo, S., Zhu, Z., Dilley, R. D., Beckmann, T., Schmidt, G. L., Dwyer, J. L., Joseph Hughes, M., & Laue, B. (2017). Cloud detection algorithm comparison and validation for operational Landsat data products. *Remote Sensing of Environment*, *194*, 379–390. https://doi.org/10.1016/J.RSE.2017.03.026

Fraser, R., Olthof, I., Kokelj, S., Lantz, T., Lacelle, D., Brooker, A., Wolfe, S., & Schwarz, S. (2014). Detecting Landscape Changes in High Latitude Environments Using Landsat Trend Analysis: 1. Visualization. *Remote Sensing*, *6*(11), 11533–11557. https://doi.org/10.3390/rs61111533

French, T. D., Houben, A. J., Desforges, J. P. W., Kimpe, L. E., Kokelj, S. V., Poulain, A. J., Smol, J. P., Wang, X., & Blais, J. M. (2014). Dissolved organic carbon thresholds affect mercury bioaccumulation in Arctic lakes. *Environmental Science and Technology*, *48*(6), 3162–3168. https://doi.org/10.1021/es403849d

Fu, B., Yang, W., Yao, H., He, H., Lan, G., Gao, E., Qin, J., Fan, D., & Chen, Z. (2022). Evaluation of spatio-temporal variations of FVC and its relationship with climate change using GEE and Landsat images in Ganjiang River Basin. *Https://Doi-Org.Proxy.Bib.Uottawa.ca/10.1080/10106049.2022.2082551*. https://doi.org/10.1080/10106049.2022.2082551

Fulton, R. J. (1989). *Quaternary Geology of Canada and Greenland* (R. J. (Robert J. Fulton (ed.)) [Book]. Canadian Government Publishing Centre, Supply and Services Canada.

Furgal, C., & Prowse, T. D. (2008). Northern Canada. In D. S. Lemmen, F. J. Warren, J. Lacroix, & E. Bush (Eds.), *From Impacts to Adaptation: Canada in a Changing Climate* (pp. 57–118). Government of Canada. https://www.nrcan.gc.ca/sites/www.nrcan.gc.ca/files/earthsciences/pdf/assess/2007/pdf/full-complet_e.pdf

Gao, H., Nie, N., Zhang, W., & Chen, H. (2020). Monitoring the spatial distribution and changes in permafrost with passive microwave remote sensing. *ISPRS Journal of Photogrammetry and Remote Sensing*, *170*. https://doi.org/10.1016/j.isprsjprs.2020.10.011

Geological Survey of Canada. (2022). *Ground Ice Map of Canada*. Natural Resources Canada. https://geoscan.nrcan.gc.ca/starweb/geoscan/servlet.starweb?path=geoscan/fulle.web&search1=R=330294

Gholizadeh, M. H., Melesse, A. M., & Reddi, L. (2016a). A comprehensive review on water quality parameters estimation using remote sensing techniques. In *Sensors (Switzerland)*. https://doi.org/10.3390/s16081298

Gholizadeh, M. H., Melesse, A. M., & Reddi, L. (2016b). Spaceborne and airborne sensors in water quality assessment. *International Journal of Remote Sensing*, *37*. https://doi.org/10.1080/01431161.2016.1190477

Gilg, O., Kovacs, K. M., Aars, J., Fort, J., Gauthier, G., Grémillet, D., Ims, R. A., Meltofte, H., Moreau, J., Post, E., Schmidt, N. M., Yannic, G., & Bollache, L. (2012). Climate change and the ecology and evolution of Arctic vertebrates. *Annals of the New York Academy of Sciences*, *1249*(1), 166–190. https://doi.org/10.1111/j.1749-6632.2011.06412.x

Gordon, H. R., & Morel, A. Y. (1983). Remote Assessment of Ocean Color for Interpretation of Satellite Visible Imagery: A Review. In *Lect. Notes Coastal Estuarine Stud.* (Vol. 4).

Graneli, W. (2012). Brownification of lakes. In F. R. W. Bengtsson L., Herschy R.W. (Ed.), *Encyclopedia of Earth Sciences Series* (pp. 117–119). Springer Netherlands. https://doi.org/10.1007/978-1-4020-4410-6_256

Grosse, G., Jones, B., & Arp, C. (2013). Thermokarst Lakes, Drainage, and Drained Basins. In J. Schroeder, R. Giardino, & J. Harbor (Eds.), *Treatise on Geomorphology* (Vol. 8, pp. 325–353). Academic Press. https://doi.org/10.1016/B978-0-12-374739-6.00216-5

Guo, X., Ye, J., & Hu, Y. (2022). Analysis of Land Use Change and Driving Mechanisms in Vietnam during the Period 2000–2020. *Remote Sensing*, *14*(7), 1600. https://doi.org/10.3390/RS14071600

Hestir, E. L., Brando, V., Campbell, G., Dekker, A., & Malthus, T. (2015). *The relationship between dissolved organic matter absorption and dissolved organic carbon in reservoirs along a temperate to tropical gradient*. https://doi.org/10.1016/j.rse.2014.09.022

Huang, H., Chen, Y., Clinton, N., Wang, J., Wang, X., Liu, C., Gong, P., Yang, J., Bai, Y., Zheng, Y., & Zhu, Z. (2017). Mapping major land cover dynamics in Beijing using all Landsat images in Google Earth Engine. *Remote Sensing of Environment*, *202*, 166–176. https://doi.org/10.1016/j.rse.2017.02.021

Huot, Y., Brown, C. A., Potvin, G., Antoniades, D., Baulch, H. M., Beisner, B. E., Bélanger, S., Brazeau, S., Cabana, H., Cardille, J. A., del Giorgio, P. A., Gregory-Eaves, I., Fortin, M. J., Lang, A. S., Laurion, I., Maranger, R., Prairie, Y. T., Rusak, J. A., Segura, P. A., … Walsh, D. A. (2019). The NSERC Canadian Lake Pulse Network: A national assessment of lake health providing science for water management in a changing climate. *Science of the Total Environment*, *695*. https://doi.org/10.1016/J.SCITOTENV.2019.133668

Hussain, M., & Mahmud, I. (2019). pyMannKendall: a python package for non parametric Mann Kendall family of trend tests. *Journal of Open Source Software*, *4*(39), 1556. http://dx.doi.org/10.21105/joss.01556

IOCCG. (2000). Remote Sensing of Ocean Colour in Coastal, and Other Optically-Complex, Waters. In S. Sathyendranath (Ed.), *Reports of the International Ocean-Colour Coordinating Group* (No. 3). IOCCG.

IPCC. (2019). *IPCC Special Report on the Ocean and Cryosphere in a Changing Climate* (H.-O. Pörtner, D. C. Roberts, V. Masson-Delmotte, P. Zhai, M. Tignor, E. Poloczanska, K. Mintenbeck, A. Alegría, M. Nicolai, A. Okem, J. Petzold, B. Rama, & N. M. Weyer (eds.)). Cambridge University Press. https://doi.org/10.1017/9781009157964.

Jin, Y., Liu, X., Chen, Y., & Liang, X. (2018). *International Journal of Remote Sensing Land-cover mapping using Random Forest classification and incorporating NDVI time-series and texture: a case study of central Shandong Land-cover mapping using Random Forest classification and incorporating NDVI time-series and texture: a case study of central Shandong*. https://doi.org/10.1080/01431161.2018.1490976

Joly, K., Jandt, R. R., & Klein, D. R. (2009). *Decrease of lichens in Arctic ecosystems: the role of wildfire, caribou, reindeer, competition and climate in north-western Alaska*. https://doi.org/10.1111/j.1751-8369.2009.00113.x

Kattsov, V. M., Kallen, E., Cattle, H., Christensen, J., Drange, H., Hanssen-Bauer, I., Johannesen, T., Karol, I., Raisanen, J., Svensson, G., & Vavulin, S. (2005). Arctic Climate Impact Assessment. In *Arctic Climate Impact Assessment* (pp. 99–150). Cambridge University Press.

Kloiber, S. M., Brezonik, P. L., & Bauer, M. E. (2002). Application of Landsat imagery to regional-scale assessments of lake clarity. In *Water Research* (Vol. 36).

Kokelj, S. V, Jenkins, R. E., Milburn, D., Burn, C. R., & Snow, N. (2005). *The Influence of Thermokarst Disturbance on the Water Quality of Small Upland Lakes, Mackenzie Delta Region, Northwest Territories, Canada*. *16*, 343–353. https://doi.org/10.1002/ppp.536

Kutser, T., Herlevi, A., Kallio, K., & Arst, H. (2001). A hyperspectral model for interpretation of passive optical remote sensing data from turbid lakes. *Science of the Total Environment*, *268*(1–3). https://doi.org/10.1016/S0048-9697(00)00682-3

Kutser, T., Pierson, D. C., Kallio, K. Y., Reinart, A., & Sobek, S. (2005). Mapping lake CDOM by satellite remote sensing. *Remote Sensing of the Environment*, *94*, 535–540. https://doi.org/10.1016/j.rse.2004.11.009

Kutser, T., & Tranvik, L. J. (2014). Using Satellite Remote Sensing to Estimate the Colored Dissolved Organic Matter Absorption Coefficient in Lakes. *Ecosystems*, *8*, 709–720. https://doi.org/10.1007/s10021-003-0148-6

Labuzzetta, C., Zhu, Z., Chang, X., & Zhou, Y. (2021). *A Submonthly Surface Water Classification Framework via Gap-Fill Imputation and Random Forest Classifiers of Landsat Imagery*. https://doi.org/10.3390/rs13091742

Lacelle, D., Fontaine, M., Forest, A. P., & Kokelj, S. (2014). High-resolution stable water isotopes as tracers of thaw unconformities in permafrost: A case study from western Arctic Canada. *Chemical Geology*, *368*, 85–96. https://doi.org/10.1016/J.CHEMGEO.2014.01.005

Larsen, A. S., O'Donnell, J. A., Schmidt, J. H., Kristenson, H. J., & Swanson, D. K. (2017). Physical and chemical characteristics of lakes across heterogeneous landscapes in arctic and subarctic Alaska. *Journal of Geophysical Research: Biogeosciences*, *122*(4), 989–1008. https://doi.org/10.1002/2016JG003729

Lathrop, R. ., & Lillesand, T. M. (1986). Use of Thematic Mapper data to assess water quality in Green Bay and central Lake Michigan. *Photogrammetric Engineering & Remote Sensing*, *52*(5), 671–680.

Lehner, B., & Döll, P. (2004). Development and validation of a global database of lakes, reservoirs and wetlands. *Journal of Hydrology*, *296*(1–4), 1–22. https://doi.org/10.1016/j.jhydrol.2004.03.028

Lewkowicz, A. G., & Way, R. G. (2019). Extremes of summer climate trigger thousands of thermokarst landslides in a High Arctic environment. *Nature Communications*, *10*(1). https://doi.org/10.1038/s41467-019-09314-7

Loiko, S. V, Pokrovsky, O. S., Raudina, T. V, Lim, A., Kolesnichenko, L. G., Shirokova, L. S., Vorobyev, S. N., & Kirpotin, S. N. (2017). Abrupt permafrost collapse enhances organic carbon, CO 2 , nutrient and metal release into surface waters. *Chemical Geology*, *471*, 153–165. https://doi.org/10.1016/j.chemgeo.2017.10.002

Matsuoka, A., Hooker, S. B., Bricaud, A., Gentili, B., & Babin, M. (2013). Estimating absorption coefficients of colored dissolved organic matter (CDOM) using a semi-analytical algorithm for southern Beaufort Sea waters: Application to deriving concentrations of dissolved organic carbon from space. *Biogeosciences*. https://doi.org/10.5194/bg-10-917-2013

Matsushita, B., Yang, W., Chang, P., Yang, F., & Fukushima, T. (2012). A simple method for distinguishing global Case-1 and Case-2 waters using SeaWiFS measurements. *ISPRS Journal of Photogrammetry and Remote Sensing*, *69*, 74–87. https://doi.org/10.1016/j.isprsjprs.2012.02.008

Matta, E., Giardino, C., Boggero, A., & Bresciani, M. (2017). Use of Satellite and In Situ Reflectance Data for Lake Water Color Characterization in the Everest Himalayan Region. *Mountain Research and Development*, *37*(1), 16–23. https://doi.org/10.1659/MRD-JOURNAL-D-15-00052.1

Matthews, M. W. (2011). A current review of empirical procedures of remote sensing in Inland and near-coastal transitional waters. In *International Journal of Remote Sensing*. https://doi.org/10.1080/01431161.2010.512947

McBean, G., Alekseev, G., Chen, D., Forland, E., Fyfe, J., Groisman, P. Y., King, R., Melling, H., Vose, R., & Whitfield, P. H. (2005). Arctic Climate: Past and Present. In *Arctic Climate Impact Assessment* (pp. 21–60). Cambridge University Press.

Militino, A., Moradi, M., & Ugarte, M. (2020). On the Performances of Trend and Change-Point Detection Methods for Remote Sensing Data. *Remote Sensing*, *12*(6), 1008. https://doi.org/10.3390/rs12061008

Millie, D. F., Moline, M. A., & Schofield, O. (2000). Optical discrimination of a phytoplankton species in natural mixed populations. *Limnology and Oceanography*, *45*(2). https://doi.org/10.4319/lo.2000.45.2.0467

Mishra, D. R., Ogashawara, I., & Gitelson, A. A. (2017). *Bio-optical Modeling and Remote Sensing of Inland Waters* (D. R. Mishra, I. Ogashawara, & A. A. Gitelson (eds.)). Elsevier.

Mobley, C. D. (1994). *Light and Water: Radiative Transfer in Natural Waters*. Academic Press.

Mobley, C. D. (2022). *The Oceanic Optics Book*. International Ocean Colour Coordinating Group (IOCCG). https://doi.org/10.25607/OBP-1710

Mobley, C. D., Stramski, D., Paul Bissett, W., & Boss, E. (2004). Optical modeling of ocean waters: Is the case 1 - case 2 classification still useful? *Oceanography*, *17*(SPL.ISS. 2). https://doi.org/10.5670/oceanog.2004.48

Moore, S. E., & Huntington, H. P. (2008). ARCTIC MARINE MAMMALS AND CLIMATE CHANGE: IMPACTS AND RESILIENCE. *Ecological Applications*, *18*(sp2), S157–S165. https://doi.org/10.1890/06-0571.1

Moquin, P. A., & Wrona, F. J. (2015). Effects of permafrost degradation on water and sediment quality and heterotrophic bacterial production of Arctic tundra lakes: An experimental approach. *Limnology and Oceanography*, *60*(5), 1484–1497. https://doi.org/10.1002/lno.10110

Morel, A. (1988). Optical modeling of the upper ocean in relation to its biogenous matter content (case I waters). *Journal of Geophysical Research*, *93*(C9). https://doi.org/10.1029/jc093ic09p10749

Morel, A., & Prieur, L. (1977). Analysis of variations in ocean color. *Limnology and Oceanography*, *22*(4). https://doi.org/10.4319/lo.1977.22.4.0709

Natural Resources Canada. (2019). *Physiographic Regions of Canada*. Government of Canada Open Government Portal. https://open.canada.ca/data/en/dataset/a3dfbaf4-1b20-4061-aa0a-e7a79953f52d

Nechad, B., Ruddick, K. G., & Park, Y. (2009). *Calibration and validation of a generic multisensor algorithm for mapping of total suspended matter in turbid waters*. *100*. https://doi.org/10.1016/j.rse.2009.11.022

Nelson, F. E., Anisimov, O. A., & Shiklomanov, N. (2001). Subsidence risk from thawing permafrost. *Nature*, *410*, 889. https://doi.org/10.1038/35073746

Nitze, I., Barrett, B., & Cawkwell, F. (2015). Temporal optimisation of image acquisition for land cover classification with random forest and MODIS time-series. *International Journal of Applied Earth Observation and Geoinformation*, *34*(1), 136–146. https://doi.org/10.1016/j.jag.2014.08.001

Nitze, I., Grosse, G., Jones, B. M., Romanovsky, V. E., & Boike, J. (2018). Remote sensing quantifies widespread abundance of permafrost region disturbances across the Arctic and Subarctic. *Nature*

Communications, *9*(1). https://doi.org/10.1038/s41467-018-07663-3

Noi Phan, T., Kuch, V., & Lehnert, L. W. (2020). Land cover classification using google earth engine and random forest classifier-the role of image composition. *Remote Sensing*, *12*(15). https://doi.org/10.3390/RS12152411

Olefeldt, D., Goswami, S., Grosse, G., Hayes, D., Hugelius, G., Kuhry, P., Mcguire, A. D., Romanovsky, V. E., Sannel, A. B. K., Schuur, E. A. G., & Turetsky, M. R. (2016). Circumpolar distribution and carbon storage of thermokarst landscapes. *Nature Communications*, *7*(13043). https://doi.org/10.1038/ncomms13043

Olmanson, L. G., Bauer, M. E., & Brezonik, P. L. (2008). A 20-year Landsat water clarity census of Minnesota's 10,000 lakes. *Remote Sensing of Environment*, *112*(11), 4086–4097. https://doi.org/10.1016/j.rse.2007.12.013

Olthof, I., Fraser, R. H., & Schmitt, C. (2015). Landsat-based mapping of thermokarst lake dynamics on the Tuktoyaktuk Coastal Plain, Northwest Territories, Canada since 1985. *Remote Sensing of Environment*, *168*. https://doi.org/10.1016/j.rse.2015.07.001

Östlund, C., Flink, P., Strömbeck, N., Pierson, D., & Lindell, T. (2001). Mapping of the water quality of Lake Erken, Sweden, from Imaging Spectrometry and Landsat Thematic Mapper. *Science of the Total Environment*. https://doi.org/10.1016/S0048-9697(00)00683-5

Pahlevan, N., Chittimalli, S. K., Balasubramanian, S. V., & Vellucci, V. (2019). Sentinel-2/Landsat-8 product consistency and implications for monitoring aquatic systems. *Remote Sensing of Environment*, *220*. https://doi.org/10.1016/j.rse.2018.10.027

Park, H., Kim, Y., & Kimball, J. S. (2016). Widespread permafrost vulnerability and soil active layer increases over the high northern latitudes inferred from satellite remote sensing and process model assessments. *Remote Sensing of Environment*, *175*. https://doi.org/10.1016/j.rse.2015.12.046

Pekel, J.-F., Cottam, A., Gorelick, N., & Belward, A. S. (2016). *High-resolution mapping of global surface water and its long-term changes Permanent New permanent Lost permanent Seasonal New seasonal Lost seasonal Seasonal to permanent Permanent to seasonal Ephemeral permanent Ephemeral seasonal*. https://doi.org/10.1038/nature20584

Previdi, M., Smith, K. L., & Polvani, L. M. (2021). Arctic amplification of climate change: a review of underlying mechanisms. *Environmental Research Letters*, *16*(9), 093003. https://doi.org/10.1088/1748-9326/AC1C29

Rantanen, M., Karpechko, A. Y., Lipponen, A., Nordling, K., Hyvärinen, O., Ruosteenoja, K., Vihma, T., & Laaksonen, A. (2022). The Arctic has warmed nearly four times faster than the globe since 1979. *Communications Earth & Environment 2022 3:1*, *3*(1), 1–10. https://doi.org/10.1038/s43247-022-00498-3

Roberts, K. E., Lamoureux, S. F., Kyser, T. K., Muir, D. C. G., Lafrenière, M. J., Iqaluk, D., Pieńkowski, A. J., & Normandeau, A. (2017). Climate and permafrost effects on the chemistry and ecosystems of High Arctic Lakes. *Scientific Reports*, *7*(1). https://doi.org/10.1038/s41598-017-13658-9

Ross, M. R. V., Topp, S. N., Appling, A. P., Yang, X., Kuhn, C., Butman, D., Simard, M., & Pavelsky, T. (2019). AquaSat: a dataset to enable remote sensing of water quality for inland waters. *Water Resources Research*, *55*. https://doi.org/10.1029/2019wr024883

Roy, D. P., Kovalskyy, V., Zhang, H. K., Vermote, E. F., Yan, L., Kumar, S. S., & Egorov, A. (2016). Characterization of Landsat-7 to Landsat-8 reflective wavelength and normalized difference vegetation index continuity. *Remote Sensing of Environment*, *185*, 57–70. https://doi.org/10.1016/J.RSE.2015.12.024

Roy, David P, Ju, J., Kline, K., Scaramuzza, P. L., Kovalskyy, V., Hansen, M., Loveland, T. R., Vermote, E., & Zhang, C. (2009). *Web-enabled Landsat Data (WELD): Landsat ETM+ composited mosaics of the conterminous United States*. https://doi.org/10.1016/j.rse.2009.08.011

Rudy, A. C. A., Lamoureux, S. F., Treitz, P., & Collingwood, A. (2013). Identifying permafrost slope disturbance using multi-temporal optical satellite images and change detection techniques. *Cold Regions Science and Technology*, *88*. https://doi.org/10.1016/j.coldregions.2012.12.008

Sargent, R. (Google/Carnegie M. U., Hancher, M. (Google), Nguyen, E. (Google), & Nourbakhsh, I. (Carnegie M. U. (2013). *Building A Visual Planetary Time Machine*. Google AI Blog. https://ai.googleblog.com/2013/06/building-visual-planetary-time-machine.html#:~:text=Some areas of,interpolated%2C original mosaics.

Schuur, E. A. G., Bockheim, J., Canadell, J. G., Euskirchen, E., Field, C. B., Goryachkin, S. V., Hagemann, S., Kuhry, P., Lafleur, P. M., Lee, H., Mazhitova, G., Nelson, F. E., Rinke, A., Romanovsky, V. E., Shiklomanov, N., Tarnocai, C., Venevsky, S., Vogel, J. G., & Zimov, S. A. (2008). Vulnerability of Permafrost Carbon to Climate Change: Implications for the Global Carbon Cycle. *BioScience*, *58*(8), 701–714. https://doi.org/10.1641/b580807

Smith, L. C., Sheng, Y., & MacDonald, G. M. (2007). A first pan-Arctic assessment of the influence of glaciation, permafrost, topography and peatlands on northern hemisphere lake distribution. *Permafrost and Periglacial Processes*, *18*(2), 201–208. https://doi.org/10.1002/ppp.581

Statistics Canada. (2016). *Provinces/territories [cartographic boundary file]*. 2016 Census - Boundary Files. . https://www12.statcan.gc.ca/census-

recensement/2011/geo/bound-limit/bound-limit-2016-eng.cfm

Stow, D. A., Hope, A., Mcguire, D., Verbyla, D., Gamon, J., Huemmrich, F., Houston, S., Racine, C., Sturm, M., Tape, K., Hinzman, L., Yoshikawa, K., Tweedie, C., Noyle, B., Silapaswan, C., Douglas, D., Griffith, B., Jia, G., Epstein, H., … Myneni, R. (2004). Remote sensing of vegetation and land-cover change in Arctic Tundra Ecosystems. *Remote Sensing of Environment*, *89*(3), 281–308. https://doi.org/10.1016/j.rse.2003.10.018

Tatsumi, K., Yamashiki, Y., Canales Torres, M. A., & Taipe, C. L. R. (2015). Crop classification of upland fields using Random forest of time-series Landsat 7 ETM+ data. *Computers and Electronics in Agriculture*, *115*, 171–179. https://doi.org/10.1016/J.COMPAG.2015.05.001

Thakur, S., Mondal, I., Bar, S., Nandi, S., Ghosh, P. B., Das, P., & De, T. K. (2021). Shoreline changes and its impact on the mangrove ecosystems of some islands of Indian Sundarbans, North-East coast of India. *Journal of Cleaner Production*, *284*, 124764. https://doi.org/10.1016/J.JCLEPRO.2020.124764

Topp, S. N., Pavelsky, T. M., Jensen, D., Simard, M., & Ross, M. R. V. (2020). Research Trends in the Use of Remote Sensing for Inland Water Quality Science: Moving Towards Multidisciplinary Applications. *Water*, *12*(1), 169. https://doi.org/10.3390/w12010169

Turetsky, M. R., Abbott, B. W., Jones, M. C., Walter Anthony, K., Olefeldt, D., Schuur, E. A. G., Koven, C., McGuire, A. D., Grosse, G., Kuhry, P., Hugelius, G., Lawrence, D. M., Gibson, C., & Sannel, A. B. K. (2019). Permafrost collapse is accelerating carbon release. In *Nature*. https://doi.org/10.1038/d41586-019-01313-4

USGS. (2019). *Landsat Collection 1 Level 1 Landsat* (Issue April). https://www.usgs.gov/media/files/landsat-collection-1-level-1-product-definition

USGS. (2020a). *Landsat 4-7 Collection 1 (C1) Surface Reflectance (LEDAPS) Product Guide* (Vol. 1, Issue August).

USGS. (2020b). *Landsat 8 Collection 1 (C1) Land Surface Reflectance Code (LaSRC) Product Guide* (Vol. 3, Issue August). https://www.usgs.gov/media/files/landsat-8-collection-1-land-surface-reflectance-code-product-guide

Van Doninck, J., & Tuomisto, H. (2017). Influence of Compositing Criterion and Data Availability on Pixel-Based Landsat TM/ETM+ Image Compositing over Amazonian Forests. *IEEE Journal of Selected Topics in Applied Earth Observations and Remote Sensing*, *10*(3). https://doi.org/10.1109/JSTARS.2016.2619695

Vincent, W. F., & Laybourn-Parry, J. (2009). Polar Lakes and Rivers: Limnology of Arctic and Antarctic Aquatic Ecosystems. In *Polar Lakes and Rivers: Limnology of Arctic and Antarctic Aquatic Ecosystems* (pp. 1–352). Oxford University Press. https://doi.org/10.1093/acprof:oso/9780199213887.001.0001

Vucic, J. M., Gray, D. K., Cohen, R. S., Syed, M., Murdoch, A. D., & Sharma, S. (2020). Changes in water quality related to permafrost thaw may significantly impact zooplankton in small Arctic lakes. *Ecological Applications*, *30*(8). https://doi.org/10.1002/eap.2186

Walter, K. M., Edwards, M. E., Grosse, G., Zimov, S. A., & Chapin, F. S. (2007). Thermokarst lakes as a source of atmospheric CH4 during the last deglaciation. *Science*, *318*(5850), 633–636. https://doi.org/10.1126/science.1142924

Wang, Q., Song, K., Xiao, X., Jacinthe, P. A., Wen, Z., Zhao, F., Tao, H., Li, S., Shang, Y., Wang, Y., & Liu, G. (2022). Mapping water clarity in North American lakes and reservoirs using Landsat images on the GEE platform with the RGRB model. *ISPRS Journal of Photogrammetry and Remote Sensing*, *194*, 39–57. https://doi.org/10.1016/J.ISPRSJPRS.2022.09.014

Watanabe, S., Laurion, I., Chokmani, K., Pienitz, R., & Vincent, W. F. (2011). Optical diversity of thaw ponds in discontinuous permafrost: A model system for water color analysis. *J. Geophys. Res*, *116*, 2003. https://doi.org/10.1029/2010JG001380

Wauthy, M., Rautio, M., Christoffersen, K. S., Forsstr€, L., Laurion, I., Mariash, H. L., Peura, S., Vincent, W. F., Stanley, E., & Del Giorgio, P. (2018). SPECIAL ISSUE-LETTER Increasing dominance of terrigenous organic matter in circumpolar freshwaters due to permafrost thaw. *Limnology and Oceanography Letters*, *3*, 186–198. https://doi.org/10.1002/lol2.10063

White, J. C., Wulder, M. A., Hobart, G. W., Luther, J. E., Hermosilla, T., Griffiths, P., Coops, N. C., Hall, R. J., Hostert, P., Dyk, A., & Guindon, L. (2014). Pixel-Based Image Compositing for Large-Area Dense Time Series Applications and Science. *Canadian Journal of Remote Sensing*, *40*(3), 192–212. https://doi.org/10.1080/07038992.2014.945827

Williamson, C. E., Dodds, W., Kratz, T. K., & Palmer, M. A. (2008). Lakes and streams as sentinels of environmental change in terrestrial and atmospheric processes. In *Frontiers in Ecology and the Environment* (Vol. 6, Issue 5, pp. 247–254). John Wiley & Sons, Ltd. https://doi.org/10.1890/070140

Williamson, C. E., Overholt, E. P., Pilla, R. M., Leach, T. H., Brentrup, J. A., Knoll, L. B., Mette, E. M., & Moeller, R. E. (2015). *Ecological consequences of long-term browning in lakes OPEN*. https://doi.org/10.1038/srep18666

Woodcock, C. E., Allen, R., Anderson, M., Belward, A., Bindschadler, R., Cohen, W., Gao, F., Goward, S. N., Helder, D., Helmer, E., Nemani, R., Oreopoulos, L., Schott, J., Thenkabail, P. S., Vermote, E. F., Vogelmann, J., Wulder, M. A., & Wynne, R. (2008). Free access to landsat imagery. In *Science* (Vol. 320,

Issue 5879). https://doi.org/10.1126/science.320.5879.1011a

Wulder, M. A., Loveland, T. R., Roy, D. P., Crawford, C. J., Masek, J. G., Woodcock, C. E., Allen, R. G., Anderson, M. C., Belward, A. S., Cohen, W. B., Dwyer, J., Erb, A., Gao, F., Griffiths, P., Helder, D., Hermosilla, T., Hipple, J. D., Hostert, P., Hughes, M. J., … Zhu, Z. (2019). Current status of Landsat program, science, and applications. *Remote Sensing of Environment*, *225*, 127–147. https://doi.org/10.1016/j.rse.2019.02.015

Wulder, M. A., Masek, J. G., Cohen, W. B., Loveland, T. R., & Woodcock, C. E. (2012). Opening the archive: How free data has enabled the science and monitoring promise of Landsat. *Remote Sensing of Environment*, *122*. https://doi.org/10.1016/j.rse.2012.01.010

Zhou, Y., Dong, J., Xiao, X., Liu, R., Zou, Z., Zhao, G., & Ge, Q. (2019). Continuous monitoring of lake dynamics on the Mongolian Plateau using all available Landsat imagery and Google Earth Engine. *Science of The Total Environment*, *689*, 366–380. https://doi.org/10.1016/J.SCITOTENV.2019.06.341

Zhu, Z., Wulder, M. A., Roy, D. P., Woodcock, C. E., Hansen, M. C., Radeloff, V. C., Healey, S. P., Schaaf, C., Hostert, P., Strobl, P., Pekel, J. F., Lymburner, L., Pahlevan, N., & Scambos, T. A. (2019). Benefits of the free and open Landsat data policy. *Remote Sensing of Environment*, *224*. https://doi.org/10.1016/j.rse.2019.02.016